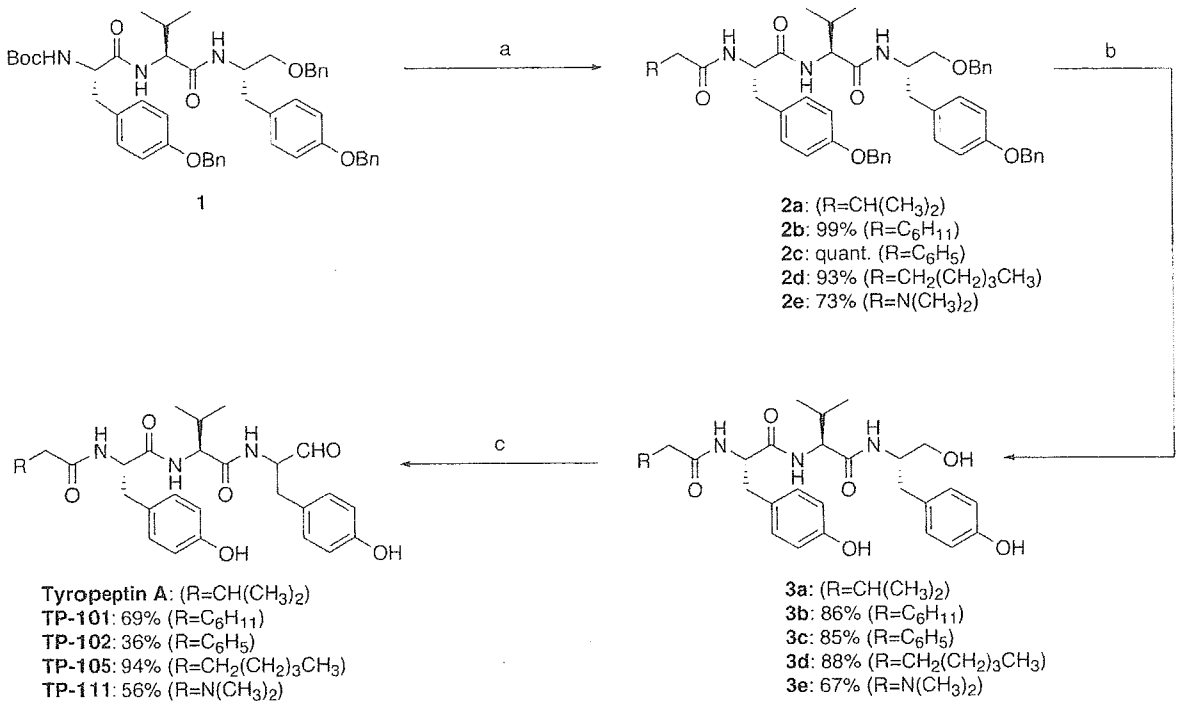

Scheme 1. Modification at the *N*-Terminal of Tyropeptin A.
(a) i. TFA, CH_2Cl_2, rt, 1 h; ii. R-CH_2COOH, WSC·HCl, HOBt, TEA, DMF, rt, 18 h; (b) H_2, Pd/C, DMF, rt, 18 h; (c) SO_3·Pyridine, TEA, DMSO, rt, 1 h.

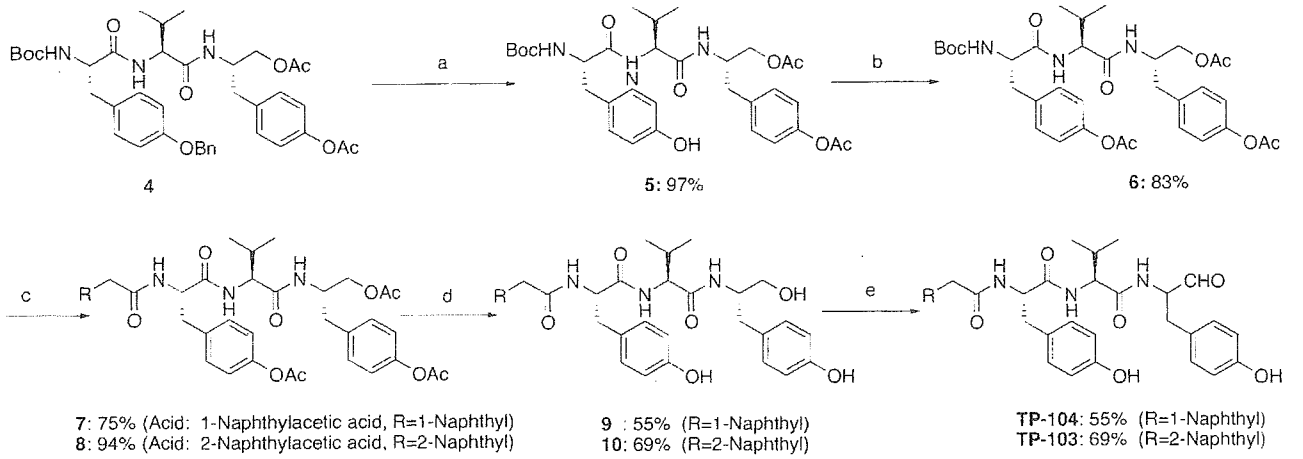

Scheme 2. Synthesis of TP-103 and TP-104.
(a) H_2, Pd/C, MeOH, EtOAc, rt, 18 h; (b) Ac_2O, pyridine, rt, 18 h; (c) i. TFA, CH_2Cl_2, rt, 1 h; ii. acid, WSC·HCl, HOBt, TEA, DMF, rt, 18 h; (d) K_2CO_3, MeOH, rt, 2 d; (e) SO_3·pyridine, TEA, DMSO, rt, 3 h.

4, having acetates and benzyl ethers as the protective groups of the alcohols (Scheme 2).

The inhibitory activities of the 20S proteasome by the tyropeptin A derivatives are summarized in Table 1. Replacement of the isopropyl group of tyropeptin A by a cyclohexyl group (TP-101) resulted in a 4-fold enhancement of its inhibitory potency for chymotrypsin-like activity compared to tyropeptin A. Aromatization of the cyclohexyl group (TP-102) resulted in a 5-fold enhancement of its inhibitory potency for chymotrypsin-like activity compared to tyropeptin A. Moreover, TP-103, having two aromatic rings (*i.e.*, a 2-naphthyl group), exhibited 10-fold enhancement of its inhibitory potency for chymotrypsin-like activity. The inhibitory activity of TP-104 having a 1-naphthyl group was stronger than that of TP-103 having a 2-naphthyl group. TP-105 having a pentyl group, however, showed lower inhibitory activity than TP-104. The most potent compound for the chymotrypsin-like activity was the 1-naphthyl derivative, TP-104, which exhibited 20-fold enhancement of its inhibitory potency for chymotrypsin-like activity compared to tyropeptin A. The structural model

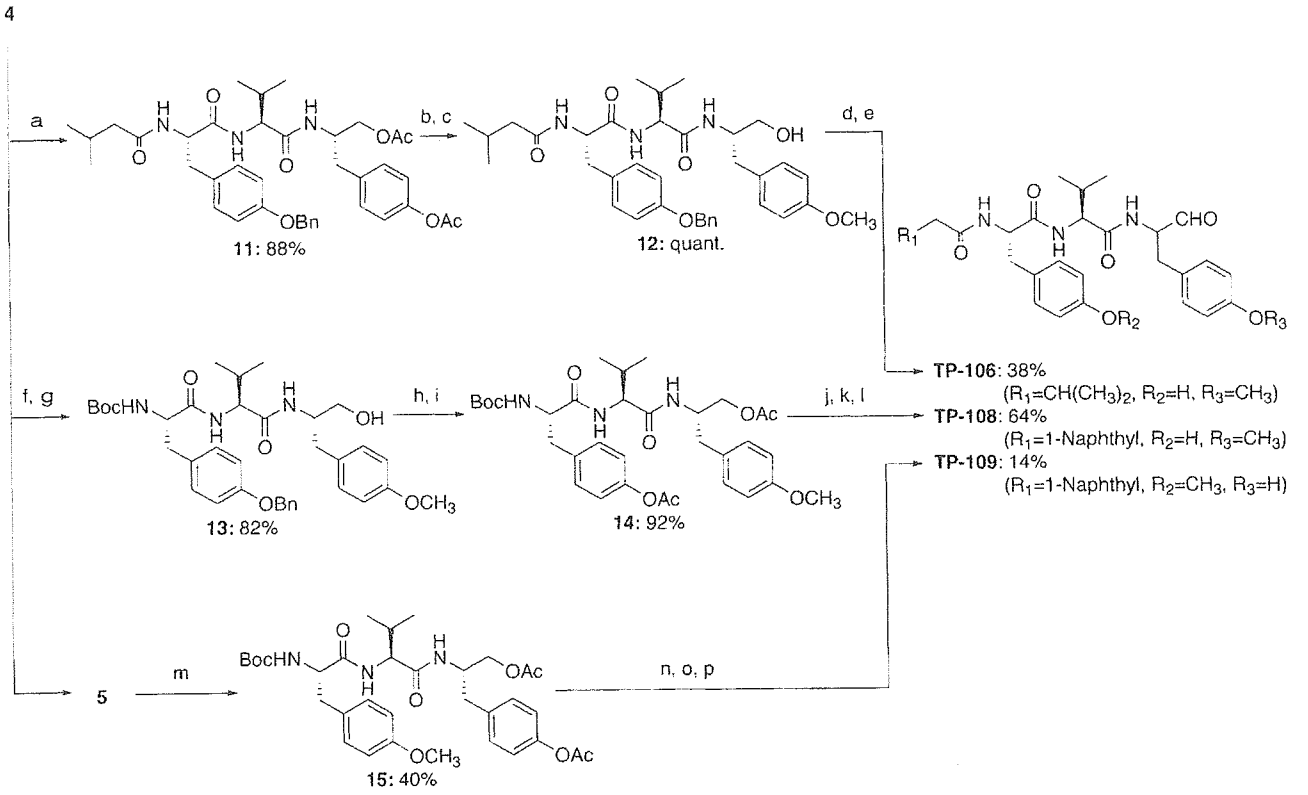

Scheme 3. Synthesis of *O*-Methyl Derivatives of Tyropeptin A.

(a) i. TFA, CH_2Cl_2, rt, 1 h; ii. isovaleric acid, WSC·HCl, HOBt, TEA, DMF, rt, 18 h; (b) K_2CO_3, MeOH, rt, 18 h; (c) $TMSCHN_2$, DIEA, $CHCl_3$, MeOH, rt, 24 h; (d) H_2, Pd/C, MeOH, rt, 3 d; (e) SO_3·pyridine, TEA, DMSO, rt, 3 h; (f) K_2CO_3, MeOH, rt, 2 d; (g) $TMSCHN_2$, DIEA, $CHCl_3$, MeOH, rt, 3 d; (h) H_2, Pd/C, MeOH, rt, 18 h; (i) Ac_2O, pyridine, rt, 18 h; (j) i. TFA, CH_2Cl_2, rt, 1 h; ii. 1-naphthylacetic acid, WSC·HCl, HOBt, TEA, DMF, rt, 18 h; (k) K_2CO_3, MeOH, rt, 18 h; (l) SO_3·pyridine, TEA, DMSO, rt, 3 h; (m) $TMSCHN_2$, DIEA, $CHCl_3$, MeOH, rt, 24 h; (n) i. TFA, CH_2Cl_2, rt, 1 h; ii. 1-naphthylacetic acid, WSC·HCl, HOBt, TEA, DMF, rt, 18 h; (o) K_2CO_3, MeOH, rt, 18 h; (p) SO_3·pyridine, TEA, DMSO, rt, 3 h.

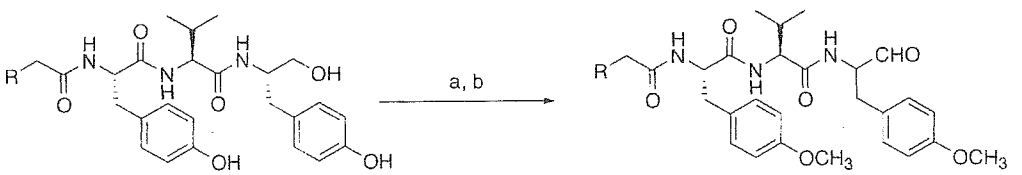

Scheme 4. Synthesis of di-*O*-Methyl Derivatives of Tyropeptin A.

(a) $TMSCHN_2$, DIEA, MeOH, $CHCl_3$; (b) SO_3·pyridine, TEA, DMSO.

of TP-104 bound to the site responsible for the chymotrypsin-like activity of mammalian 20S proteasome revealed that the increased inhibitory potency of TP-104 would have come from the increased affinity for the active site.[12] Additionally, TP-104 allowed enhancement of the inhibitory potency for a digestive enzyme such as α-chymotrypsin (Table 1).

In order to examine the role of the phenolic hydroxyl groups in the inhibitory activity against 20S proteasome, the *O*-methyl derivatives (TP-106, TP-107, TP-108, TP-109 and TP-110) were synthesized, as illustrated in Schemes 3 and 4. The *O*-methylated derivatives of tyropeptin A, TP-106 and TP-107, inhibited the chymotrypsin-like activity of the 20S proteasome to the same extent as tyropeptin A (Table 1). In contrast, their inhibitory activities against the trypsin-like activity of 20S proteasome were decreased. We therefore attempted to improve the selectivity for inhibition of the 20S proteasome activity of TP-104 by *O*-methylation. TP-108, TP-109 and TP-110 showed slightly lower inhibitory activities for the chymotrypsin-like activity compared to TP-104. However, these compounds markedly decreased the inhibition of trypsin-like activity. Notably, TP-110 did not inhibit the trypsin-like and PGPH activities, even at the concentration of 100 μM. These results indicate that *O*-methylation of the tyropeptins

Table 1. Inhibitory Activities of the 20S Proteasome and α-Chymotrypsin by Tyropeptin A Derivatives

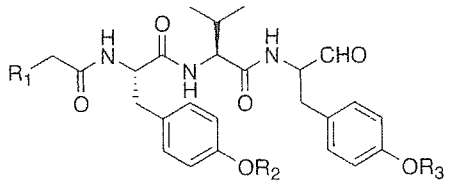

Compound	R_1	R_2	R_3	IC_{50} (μM)			
				20S proteasome			α-Chymotrypsin
				Chymotrypsin-like activity	PGPH activity	Trypsin-like activity	
Tyropeptin A	$CH(CH_3)_2$	H	H	0.14	68	5	2.3
TP-101	C_6H_{11}	H	H	0.033	17	3	2.7
TP-102	C_6H_5	H	H	0.027	16	2	0.31
TP-103	2-Naphthyl	H	H	0.014	4.7	0.7	0.27
TP-104	1-Naphthyl	H	H	0.007	4.9	1.2	0.084
TP-105	$CH_2(CH_2)_3CH_3$	H	H	0.037	20	2	1.7
TP-106	$CH(CH_3)_2$	H	CH_3	0.19	21	21	19
TP-107	$CH(CH_3)_2$	CH_3	CH_3	0.12	56	37	52
TP-108	1-Naphthyl	H	CH_3	0.018	38	6	5.7
TP-109	1-Naphthyl	CH_3	H	0.020	31	6	0.31
TP-110	1-Naphthyl	CH_3	CH_3	0.027	>100	>100	24
TP-111	$N(CH_3)_2$	H	H	1.2	>100	7.8	>40
MG132				0.068	1.4	4.5	>100

Table 2. Growth Inhibitory Activities of the Tyropeptin A Derivatives

Compound	IC_{50} (μM)			
	RPMI8226	SW-480	HT-1080	RKO
Tyropeptin A	4.1	4.5	9.8	7.8
TP-101	0.27	0.36	1.5	1.2
TP-102	1.2	2.0	5.9	4.9
TP-103	0.87	1.6	3.0	1.8
TP-104	0.20	0.27	0.72	0.35
TP-105	0.33	0.74	1.5	1.2
TP-106	0.68	1.9	2.1	1.3
TP-107	0.30	1.3	2.4	0.57
TP-108	0.062	0.21	0.38	0.084
TP-109	0.021	0.087	0.22	0.059
TP-110	0.012	0.059	0.11	0.014
TP-111	>20	>20	>20	>20
MG132	1.5	2.3	6.5	1.7

Cells were incubated with a test sample for 72 hours, and cell growth was determined by the MTT method.

enhanced the specificity for inhibition of the chymotrypsin-like activity of the 20S proteasome. We found that TP-110 specifically inhibited the chymotrypsin-like activity of the 20S proteasome and varied in its inhibitory selectivity from tyropeptin A or the known proteasome inhibitor MG132.[6,13] Additionally, *O*-methylation of the tyropeptins attenuated the inhibitory activity for α-chymotrypsin activity, and TP-110 hardly inhibited the α-chymotrypsin activity.

The growth inhibitory activities of the tyropeptin A derivatives against various cancer cell lines are summarized in Table 2. Enhancement of the proteasome inhibitory activity enhanced the growth inhibitory activity. Moreover, *O*-methylation of the tyropeptins exhibited an effective increase in the growth inhibitory activity. It is likely that the *O*-methyl derivatives might be efficiently incorporated into cells, because of the enhanced hydrophobicity by *O*-methylation. TP-110 was the most potent compound among the synthesized tyropeptins. Although tyropeptin A weakly inhibited the growth of various cell lines, TP-110 strongly inhibited the growth of the cells.

We successfully obtained two compounds. The most potent compound, TP-104, exhibited a 20-fold inhibitory potency enhancement for the chymotrypsin-like activity of 20S proteasome compared to tyropeptin A. TP-110 specifically inhibited the chymotrypsin-like activity of the 20S proteasome and had strong activity toward cell growth inhibition. Thus, such proteasome inhibitor as TP-104 and TP-110 might be useful for the treatment of cancer, inflammatory diseases and other diseases. An evaluation on the anticancer activity of these compounds will be reported elsewhere.

Experimental

NMR spectra were obtained with a JEOL JNM-A 500 spectrometer at 500 MHz and a JEOL JNM-EX 400 spectrometer at 400 MHz. UV absorption spectra were determined with a HITACHI U-3210 spectrophotometer, IR absorption spectra were determined with a HORIBA FT-210 spectrometer, and FAB-MS and HRFAB-MS data were measured with a JEOL JMS-SX 102 spectrometer. APCI-MS data were measured with a HITACHI M-1200H spectrometer, and optical rotation data were determined with a Perkin-Elmer 241 polarimeter.

Chemical synthesis. We had previously synthesized tyropeptin A in order to determine the structures,[10] and various tyropeptin A derivatives were synthesized by a similar procedure. The synthetic routes to the tyropeptin A derivatives modified in the *N*-terminal group are shown in Schemes 1 and 2, while the preparation procedures for the *O*-methyl derivatives of tyropeptin A and TP-104 are illustrated in Schemes 3 and 4. An aldehyde group was observed as a methyl hemiacetal in the NMR spectrum of each compound in CD_3OD.

Cyclohexylacetyl-L-tyrosyl-L-valyl-DL-tyrosinal (TP-101). TP-101 was synthesized by a similar procedure to that for tyropeptin A in a 59% yield from **1**. Mp 153–155 °C. $[\alpha]_D^{25}$ −33.3° (*c* 0.33, MeOH). Rf 0.32 ($CHCl_3$/MeOH = 10/1). APCI-MS *m/z*: 552 $(M+H)^+$, 550 $(M-H)^-$. HRFAB-MS *m/z*: calcd. for $C_{31}H_{42}O_6N_3$, 552.3074; found, 552.3082 $(M+H)^+$. IR (KBr) ν_{max} cm^{-1}: 3280, 2930, 1730, 1640, 1540, 1515, 1230, 825. ^{1}H-NMR (400 MHz, CD_3OD) δ: 0.64–0.83 (2H, m, cyclohexyl-H_2), 0.86 (3H, d, J = 7.2 Hz, CH_3), 0.88 (3H, d, J = 7.2 Hz, CH_3), 1.10–1.65 (9H, m, cyclohexyl-H_9), 1.97 (1H, m, Val-β-H), 1.98 (2H, d, J = 7.0 Hz, CH_2CO), 2.62 (1H, m, Tyral-β-H), 2.72 (1H, m, Tyr-β-H), 2.89 (1H, m, Tyral-β-H), 2.99 (1H, dd, J = 4.4, 14.4 Hz, Tyr-β-H), 4.05 (1H, m, Tyral-α-H), 4.12 (1H, dd, J = 3.4, 7.4 Hz, Val-α-H), 4.44 (1H, dd, J = 4.0, 7.2 Hz, hemiacetal-H), 4.60 (1H, ddd, J = 2.8, 4.4, 10.4 Hz, Tyr-α-H), 6.66 (2H, d, J = 8.4 Hz, Tyr-ε-H × 2), 6.67 (2H, d, J = 8.4 Hz, Tyral-ε-H × 2), 7.02 (2H, d, J = 8.4 Hz, Tyral-δ-H × 2), 7.05 (2H, d, J = 8.4 Hz, Tyr-δ-H × 2). ^{13}C-NMR (100 MHz, CD_3OD) δ: 18.6 (CH_3), 19.7 (CH_3), 27.2 (cyclohexyl-CH_2), 27.3 (cyclohexyl-CH_2), 27.3 (cyclohexyl-CH_2), 32.2 (Val-β-CH), 33.9 (cyclohexyl-CH_2), 34.1 (cyclohexyl-CH_2), 35.3 (Tyral-β-CH_2), 36.9 (cyclohexyl-CH), 37.8 (Tyr-β-CH_2), 44.9 (CH_2CO), 56.0 (Tyral-α-CH), 56.6 (Tyr-α-CH), 60.2 (Val-α-CH), 98.8 (hemiacetal-C), 116.2 (Tyr-ε-CH), 116.2 (Tyral-ε-CH), 129.4 (Tyr-γ-C), 130.4 (Tyral-γ-C), 131.3 (Tyr-δ-CH), 131.4 (Tyral-δ-CH), 156.9 (Tyral-ζ-C), 157.3 (Tyr-ζ-C), 173.2 (Val-CO), 173.9 (Tyr-CO), 175.5 (CH_2CO).

Phenylacetyl-L-tyrosyl-L-valyl-DL-tyrosinal (TP-102). TP-102 was synthesized by a similar procedure to that for tyropeptin A in a 31% yield from **1**. Mp 103–107 °C. $[\alpha]_D^{26}$ −37.4° (*c* 0.27, MeOH). Rf 0.29 ($CHCl_3$/MeOH = 10/1). APCI-MS *m/z*: 546 $(M+H)^+$, 544 $(M-H)^-$. HRFAB-MS *m/z*: calcd. for $C_{31}H_{36}O_6N_3$, 546.2604; found, 546.2625 $(M+H)^+$. IR (KBr) ν_{max} cm^{-1}: 3300, 2960, 1730, 1640, 1550, 1515, 1240, 830. ^{1}H-NMR (400 MHz, CD_3OD) δ: 0.81 (3H, d, J = 6.8 Hz, CH_3), 0.85 (3H, dd, J = 2.0, 6.8 Hz, CH_3), 1.92–2.00 (1H, m, Val-β-H), 2.62 (1H, m, Tyral-β-H), 2.74 (1H, ddd, J = 2.3, 10.1, 14.2 Hz, Tyr-β-H), 2.89 (1H, m, Tyral-β-H), 2.98 (1H, dd, J = 4.6, 14.2 Hz, Tyr-β-H), 3.45 (2H, d, J = 12.4 Hz, CH_2CO), 4.04 (1H, m, Tyral-α-H), 4.10 (1H, dd, J = 2.8, 7.2 Hz, Val-α-H), 4.43 (1H, dd, J = 4.2, 6.6 Hz, hemiacetal-H), 4.60 (1H, m, Tyr-α-H), 6.64 (2H, d, J = 8.0 Hz, Tyr-ε-H × 2), 6.65 (2H, d, J = 8.0 Hz, Tyral-ε-H × 2), 6.96–7.08 (5H, m, Ph-H_5), 7.21 (4H, d, J = 8.0 Hz, Tyr-δ-H × 2, Tyral-δ-H × 2). ^{13}C-NMR (100 MHz, CD_3OD) δ: 18.6 (CH_3), 19.7 (CH_3), 32.2 (Val-β-CH), 35.4 (Tyral-β-CH_2), 37.8 (Tyr-β-CH_2), 43.6 (CH_2CO), 56.1 (Tyral-α-CH), 56.7 (Tyr-α-CH), 60.3 (Val-α-CH), 98.7 (hemiacetal-H), 116.2 (Tyr-ε-CH), 116.3 (Tyral-ε-CH), 127.9 (Ph-CH), 129.1 (Tyr-γ-C), 129.6 (Ph-CH), 130.1 (Ph-CH), 130.5 (Tyral-δ-CH), 131.3 (Tyr-δ-CH), 131.4 (Tyral-δ-CH), 136.6 (Ph-C), 156.8 (Tyral-ζ-C), 157.3 (Tyr-ζ-C), 173.1 (Val-CO), 173.6 (CH_2CO), 174.0 (Tyr-CO).

Heptanoyl-L-tyrosyl-L-valyl-DL-tyrosinal (TP-105). TP-105 was synthesized by a similar procedure to that for tyropeptin A in a 77% yield from **1**. Mp 135–142 °C. $[\alpha]_D^{25}$ −32.6° (*c* 0.38, MeOH). Rf 0.32 ($CHCl_3$/MeOH = 10/1). APCI-MS *m/z*: 540 $(M+H)^+$, 538 $(M-H)^-$. HRFAB-MS *m/z*: calcd. for $C_{30}H_{42}O_6N_3$, 540.3074; found, 540.3080 $(M+H)^+$. IR (KBr) ν_{max} cm^{-1}: 3280, 2960, 1730, 1640, 1540, 1515, 1230, 825. ^{1}H-NMR (400 MHz, CD_3OD) δ: 0.86 (3H, d, J = 6.8 Hz, CH_3), 0.87 (3H, t, J = 6.8 Hz, CH_3), 0.88 (3H, d, J = 6.8 Hz, CH_3), 1.10–1.30 (6H, m, $CH_3CH_2(CH_2)_3$), 1.45 (2H, m, CH_3CH_2), 1.95 (1H, m, Val-β-H), 2.12 (2H, t, J = 7.4 Hz, CH_2CO), 2.62 (1H, m, Tyral-β-H), 2.72 (1H, m, Tyr-β-H), 2.89 (1H, m, Tyral-β-H), 2.98 (1H, dd, J = 4.4, 14.0 Hz, Tyr-β-H), 4.04 (1H, m, Tyral-α-H), 4.12 (1H, m, Val-α-H), 4.43 (1H, dd, J = 4.0, 6.8 Hz, hemiacetal-H), 4.58 (1H, m, Tyr-α-H), 6.60–6.70 (4H, m, Tyr-ε-H × 2, Tyral-ε-H × 2), 6.99–7.08 (4H, m, Tyr-δ-H × 2, Tyral-δ-H × 2). ^{13}C-NMR (100 MHz, CD_3OD) δ: 14.4 (CH_3), 18.6 (CH_3), 19.7 (CH_3), 23.6 (Heptanoyl-CH_2), 27.0 (Heptanoyl-CH_2), 29.8 (Heptanoyl-CH_2), 32.2 (Val-β-CH), 32.7 (Heptanoyl-CH_2), 35.3 (Tyral-β-CH_2), 36.9 (Heptanoyl-CH_2), 37.8 (Tyr-β-CH_2), 56.0 (Tyral-α-CH), 56.6 (Tyr-α-CH), 60.2 (Val-α-CH), 98.7 (hemiacetal-C), 116.2 (Tyr-ε-CH, Tyral-ε-CH), 129.3 (Tyr-γ-C), 130.4 (Tyral-γ-C), 131.3 (Tyr-δ-CH), 131.4 (Tyral-δ-CH), 156.8 (Tyral-ζ-C), 157.2 (Tyr-ζ-CH), 173.1 (Val-CO), 173.9 (Tyr-CO), 176.3 (CH_2CO).

N,N-Dimethyl-glycyl-L-tyrosyl-L-valyl-DL-tyrosinal (TP-111). TP-111 was synthesized by a similar procedure to that for tyropeptin A in a 27% yield from **1**. Mp 104–108 °C. $[\alpha]_D^{24}$ −18.2° (*c* 0.55, MeOH). Rf 0.1 ($CHCl_3$/MeOH = 10/1). APCI-MS *m/z*: 513 $(M+H)^+$, 511 $(M-H)^-$. HRFAB-MS *m/z*: calcd. for $C_{27}H_{37}O_6N_4$, 513.2713; found, 513.2712 $(M+H)^+$. IR (KBr) ν_{max} cm^{-1}: 3290, 2960, 1720, 1640, 1550, 1520, 1240, 830. ^{1}H-NMR (400 MHz, CD_3OD) δ: 0.64 (3H, d, J = 6.8 Hz, CH_3), 0.88 (3H, d, J = 6.8 Hz, CH_3), 1.99 (1H, m, Val-β-H), 2.20 (6H, s, $N(CH_3)_2$), 2.62 (1H, m, Tyral-β-H), 2.78 (1H, dd, J = 9.0, 14.0 Hz, Tyr-β-H), 2.94 (1H, dd, J = 4.0, 15.0 Hz, Tyral-β-H), 3.02 (1H, d, J = 14.0 Hz, Tyral-β-H), 3.47 (1H, d, J = 5.6 Hz, Gly-α-H), 4.05 (1H, m, Tyral-α-H), 4.10 (1H, d, J = 5.6 Hz, Gly-α-H), 4.12 (1H, d, J = 7.2 Hz, Val-α-H), 4.48 (1H, dd, J = 3.6, 5.6 Hz, hemiacetal-H), 4.62 (1H, m, Tyr-α-H), 6.64–6.72 (4H, m, Tyr-ε-H × 2, Tyral-ε-H × 2),

7.00–7.08 (4H, m, Tyr-δ-*H* × 2, Tyral-δ-*H* × 2). ^{13}C-NMR (100 MHz, CD_3OD) δ: 18.7 (CH_3), 19.7 (CH_3), 32.2 (Val-β-*C*H), 34.8 (Tyral-β-CH_2), 37.0 (Gly-α-CH_2), 38.1 (Tyr-β-CH_2), 45.8 (N(CH_3)$_2$), 55.6 (Tyral-α-*C*H), 56.6 (Tyr-α-*C*H), 60.1 (Val-α-*C*H), 98.7 (hemiacetal-*C*), 116.1 (Tyr-ε-*C*H), 116.2 (Tyral-ε-*C*H), 128.8 (Tyr-γ-*C*), 130.4 (Tyral-γ-*C*), 131.1 (Tyr-δ-*C*H), 131.2 (Tyral-δ-*C*H), 156.8 (Tyral-ζ-*C*), 157.3 (Tyr-ζ-*C*), 172.0 (Gly-*C*O), 173.0 (Val-*C*O), 173.5 (Tyr-*C*O).

Synthesis of the naphthyl derivatives.

(N-t-Butoxycarbonyl-O-benzyl)-L-tyrosyl-L-valyl-(di-O-acetyl)-L-tyrosinol (4). Compound **4** was synthesized by a similar procedure to that for (*N-t*-butoxycarbonyl-*O*-benzyl)-L-tyrosyl-L-valyl-(di-*O*-benzyl)-L-tyrosinol. In brief, (*N-t*-butoxycarbonyl)-L-tyrosinol was treated with acetic anhydride in pyridine to give (*N-t*-butoxycarbonyl-di-*O*-acetyl)-L-tyrosinol. This compound was treated with trifluoroacetic acid (TFA), and then coupled with *t*-butoxycarbonyl-L-valine in the presence of water-soluble carbodiimide hydrochloride (WSC·HCl) and 1-hydroxybenzotriazole (HOBt) to yield the dipeptide. Removal of the *t*-butoxycarbonyl group of the dipeptide and subsequent coupling with (*N-t*-butoxycarbonyl-*O*-benzyl)-L-tyrosine gave tripeptide **4**. APCI-MS *m/z* 704 $(M+H)^+$. ^{1}H-NMR (400 MHz, $CDCl_3$) δ: 0.76 (3H, d, $J = 6.8$ Hz, CH_3), 0.85 (3H, d, $J = 6.8$ Hz, CH_3), 1.41 (9H, s, C(CH_3)$_3$), 2.07 (3H, s, COCH_3), 2.16 (1H, m, Val-β-*H*), 2.26 (3H, s, COCH_3), 2.78 (2H, m, Tyrol-β-H_2), 3.03 (2H, m, Tyr-β-H_2), 4.04 (2H, d, $J = 5.2$ Hz, CHCH_2O), 4.14 (1H, m, Val-α-*H*), 4.25 (1H, m, Tyr-α-*H*), 4.42 (1H, m, Tyrol-α-*H*), 4.93 (1H, d, $J = 6.4$ Hz, N*H*), 5.02 (2H, s, OCH_2Ph), 6.41 (1H, br, N*H*), 6.48 (1H, d, $J = 8.8$ Hz, N*H*), 6.91 (2H, d, $J = 8.8$ Hz, Tyr-ε-*H* × 2), 6.99 (2H, d, $J = 8.8$ Hz, Tyrol-ε-*H* × 2), 7.11 (2H, d, $J = 8.8$ Hz, Tyr-δ-*H* × 2), 7.18 (2H, d, $J = 8.8$ Hz, Tyrol-δ-*H* × 2), 7.30–7.45 (5H, m, Ph-H_5).

(N-t-Butoxycarbonyl)-L-tyrosyl-L-valyl-(di-O-acetyl)-L-tyrosinol (5). To a solution of **4** (2.3 g, 3.3 mmol) in 30 ml of MeOH and 10 ml of EtOAc was added 230 mg of 10% palladium on charcoal (Pd/C), and the mixture was stirred under a hydrogen atmosphere for 18 h at room temperature. The catalyst was filtered off through a Celite layer, and the resulting filtrate was concentrated under reduced pressure. The residue was purified by silica gel column chromatography ($CHCl_3$/MeOH, 5:1) to give **5** (927 mg) as a white powder in a 97% yield. APCI-MS *m/z* 614 $(M+H)^+$. ^{1}H-NMR (400 MHz, $CDCl_3/CD_3OD$) δ: 0.89 (3H, d, $J = 7.2$ Hz, CH_3), 0.93 (3H, d, $J = 7.2$ Hz, CH_3), 1.39 (9H, s, C(CH_3)$_3$), 2.04 (1H, m, Val-β-*H*), 2.06 (3H, s, COCH_3), 2.25 (3H, s, COCH_3), 2.70–2.85 (3H, m, Tyrol-β-H_2, Tyr-β*H*), 2.99 (1H, dd, 5.4, 13.7 Hz, Tyr-β-*H*), 3.97 (1H, d, $J = 6.8$ Hz, Val-α-*H*), 4.09 (2H, dd, 8.2, 14.7 Hz, CHCH_2O), 4.24 (1H, m, Tyr-α-*H*), 4.37 (1H, m, Tyrol-α-*H*), 6.74 (2H, d, $J = 8.2$ Hz, Tyr-ε-*H* × 2), 7.01 (2H, d, $J = 8.2$ Hz, Tyrol-ε-*H* × 2), 7.04 (2H, d, $J = 8.2$ Hz, Tyr-δ-*H* × 2), 7.23 (2H, d, $J = 8.2$ Hz, Tyrol-δ-*H* × 2).

(N-t-Butoxycarbonyl-O-acetyl)-L-tyrosyl-L-valyl-(di-O-acetyl)-L-tyrosinol (6). To a solution of **5** (600 mg, 0.98 mmol) in 5 ml of pyridine was added 2.5 ml of acetic anhydride (26.6 mmol), and the mixture was stirred for 18 h at room temperature. The solvent was evaporated with toluene, and then the resulting residue was purified by silica gel column chromatography ($CHCl_3$) to give **6** (542 mg) as a white powder in an 83% yield. APCI-MS *m/z* 656 $(M+H)^+$. ^{1}H-NMR (400 MHz, $CDCl_3$) δ: 0.79 (3H, d, $J = 7.0$ Hz, CH_3), 0.86 (3H, d, $J = 7.0$ Hz, CH_3), 1.41 (9H, s, C(CH_3)$_3$), 2.07 (3H, m, COCH_3), 2.15 (1H, m, Val-β-*H*), 2.26 (6H, s, COCH_3 × 2), 2.76 (1H, dd, $J = 8.0$, 13.6 Hz, Tyrol-β-*H*), 2.84 (1H, dd, $J = 6.4$, 13.6 Hz, Tyrol-β-*H*), 3.09 (2H, m, Tyr-β-H_2), 4.05 (2H, d, $J = 5.2$ Hz, CHCH_2O), 4.14 (1H, t, $J = 7.8$ Hz, Val-α-*H*), 4.29 (1H, m, Tyr-α-*H*), 4.41 (1H, m, Tyrol-α-*H*), 4.98 (1H, d, $J = 7.2$ Hz, N*H*), 6.42 (1H, br, N*H*), 6.56 (1H, d, $J = 8.4$ Hz, N*H*), 7.00 (2H, d, $J = 8.2$ Hz, Tyr-ε-*H* × 2), 7.02 (2H, d, $J = 8.2$ Hz, Tyrol-ε-*H* × 2), 7.19 (2H, d, $J = 8.2$ Hz, Tyr-δ-*H* × 2), 7.20 (2H, d, $J = 8.2$ Hz, Tyrol-δ-*H* × 2).

1-Naphthylacetyl-(O-acetyl)-L-tyrosyl-L-valyl-(di-O-acetyl)-L-tyrosinol (7). To a solution of **6** (522 mg, 0.8 mmol) in 4 ml of CH_2Cl_2 was added 4 ml of TFA at 0 °C, and then the solution was stirred for 1 h at room temperature. The solvent was evaporated, and the residue was coevaporated twice with toluene. To the residue in 14 ml of CH_2Cl_2 were added 242 mg of triethylamine (TEA, 2.4 mmol), 447 mg of 1-naphthylacetic acid (2.4 mmol), 164 mg of HOBt (1.2 mmol) and 201 mg of WSC·HCl (1.1 mmol) at 0 °C. The reaction mixture was stirred for 18 h at room temperature. Then the reaction mixture was diluted with EtOAc, and successively washed with 5% aq. $NaHCO_3$, 4% aq. citric acid and H_2O. The organic layer was dried over Na_2SO_4 and concentrated under reduced pressure. The residue was purified by silica gel column chromatography ($CHCl_3$) to give **7** (300 mg) as a white solid in a 75% yield. APCI-MS *m/z* 724 $(M+H)^+$. ^{1}H-NMR (400 MHz, $CDCl_3$) δ: 0.74 (3H, d, $J = 6.8$ Hz, CH_3), 0.81 (3H, d, $J = 6.8$ Hz, CH_3), 1.93 (1H, m, Val-β-*H*), 2.05 (3H, s, COCH_3), 2.24 (3H, s, COCH_3), 2.28 (3H, s, COCH_3), 2.75–2.80 (3H, m, Tyrol-β-H_2, Tyr-β-*H*), 2.88 (1H, dd, $J = 5.4$, 14.2 Hz, Tyr-β-*H*), 3.95 (2H, d, $J = 7.2$ Hz, CHCH_2O), 3.98 (2H, s, CH_2CO), 4.07 (1H, dd, $J = 4.4$, 11.2 Hz, Val-α-*H*), 4.37 (1H, m, Tyrol-α-*H*), 4.59 (1H, dd, $J = 7.9$, 13.2 Hz, Tyr-β-*H*), 6.48 (1H, d, $J = 8.0$ Hz, N*H*), 6.75 (2H, d, $J = 8.6$ Hz, Tyr-ε-H_2 × 2), 6.78 (2H, d, $J = 8.6$ Hz, Tyrol-ε-H_2 × 2), 6.97 (2H, d, $J = 8.6$ Hz, Tyr-δ-H_2 × 2), 7.19 (2H, d, $J = 8.6$ Hz, Tyrol-δ-H_2 × 2), 7.32 (1H, d, $J = 7.2$, naphthyl-*H*), 7.43 (1H, d, $J = 7.6$ Hz, naphthyl-*H*), 7.49 (2H, m, naphthyl-H_2), 7.81–7.90 (3H, m, naphthyl-H_3).

1-Naphthylacetyl-L-tyrosyl-L-valyl-L-tyrosinol (9). To a solution of **7** (293 mg, 0.4 mmol) in 15 ml of MeOH was added 300 mg of K_2CO_3 (2.17 mmol), and then the solution was stirred for 2 days at room temperature. The solvent was evaporated, and the residue was diluted with

EtOAc, and successively washed with 5% aq. $NaHCO_3$, 4% aq. citric acid and H_2O. The organic layer was dried over Na_2SO_4 and concentrated under reduced pressure. The residue was purified by silica gel column chromatography ($CHCl_3$/MeOH, 25:1) to give **9** (184 mg) as a white solid in a 55% yield. APCI-MS *m/z* 598 $(M+H)^+$. ^{1}H-NMR (400 MHz, CD_3OD) δ: 0.78 (3H, d, $J = 6.8$ Hz, C*H*$_3$), 0.83 (3H, d, $J = 6.8$ Hz, C*H*$_3$), 1.93 (1H, m, Val-β-*H*), 2.61 (1H, dd, $J = 7.6$, 14.0 Hz, Tyrol-β-*H*), 2.76 (2H, m, Tyrol-β-*H*), 2.95 (1H, dd, $J = 5.0$, 14.0 Hz, Tyr-β-*H*), 3.45 (2H, d, $J = 5.2$ Hz, CHC*H*$_2$O), 3.97 (2H, s, C*H*$_2$CO), 4.01 (1H, m, Tyrol-α-*H*), 4.08 (1H, d, $J = 7.2$ Hz, Val-α-*H*), 4.62 (1H, dd, $J = 4.8$, 9.2 Hz, Tyr-α-*H*), 6.59 (2H, d, $J = 8.4$ Hz, Tyr-ε-*H* × 2), 6.66 (2H, d, $J = 8.4$ Hz, Tyrol-ε-*H* × 2), 6.89 (2H, d, $J = 8.4$ Hz, Tyr-δ-*H* × 2), 7.01 (2H, d, $J = 8.4$ Hz, Tyrol-δ-*H* × 2), 7.25 (1H, d, $J = 6.4$ Hz, naphthyl-*H*), 7.38 (1H, t, $J = 7.6$ Hz, naphthyl-*H*), 7.45 (2H, m, naphthyl-*H*$_2$), 7.75–7.88 (3H, m naphthyl-*H*$_3$).

1-Naphthylacetyl-L-tyrosyl-L-valyl-DL-tyrosinal (TP-104). To a solution of **9** (76 mg, 0.13 mmol) in 0.8 ml of DMSO was added 51 mg of TEA (0.51 mmol) at room temperature, and the solution was stirred for 5 minutes at 0 °C. An 81 mg amount of a sulfur trioxide-pyridine complex (SO_3·pyridine, 0.51 mmol) in 0.8 ml of DMSO was added to the reaction mixture at 0 °C, and the solution was stirred for an additional 3 h at room temperature. The reaction mixture was diluted with EtOAc, and successively washed with 4% aq. citric acid, H_2O, 5% aq. $NaHCO_3$ and brine. The organic layer was dried over Na_2SO_4 and concentrated under reduced pressure. The residue was purified by silica gel column chromatography ($CHCl_3$/MeOH, 25:1) to give TP-104 (74 mg) as a white powder in a 55% yield. Mp 154–156 °C. $[\alpha]_D^{23}$ −18.2° (*c* 0.33, MeOH). Rf 0.45 ($CHCl_3$/MeOH = 10/1). APCI-MS *m/z*: 596 $(M+H)^+$, 594 $(M-H)^-$. HRFAB-MS *m/z*: calcd. for $C_{35}H_{38}O_6N_3$, 596.2761; found, 596.2764 $(M+H)^+$. IR (KBr) ν_{max} cm^{-1}: 3410, 3290, 1720, 1640, 1540, 1520, 1230, 780. ^{1}H-NMR (400 MHz, $CDCl_3/CD_3OD$) δ: 0.74 (3H, dd, $J = 3.2$, 6.6 Hz, C*H*$_3$), 0.81 (3H, dd, $J = 3.2$, 6.6 Hz, C*H*$_3$), 1.94 (1H, m, Val-β-*H*), 2.63–2.79 (2H, m, Tyr-β-*H*, Tyral-β-*H*), 2.84–2.91 (2H, m, Tyr-β-*H*, Tyral-β-*H*), 3.97 (2H, s, C*H*$_2$CO), 4.03 (1H, dd, $J = 6.8$, 9.2 Hz, Tyral-α-*H*), 4.13 (1H, m, Val-α-*H*), 4.42 (1H, d, $J = 2.4$ Hz, hemiacetal-*H*), 4.55 (1H, m, Tyr-α-*H*), 6.56 (2H, t, $J = 8.4$ Hz, Tyr-ε-*H* × 2), 6.71 (4H, t, $J = 8.4$ Hz, Tyr-ε-*H* × 2, Tyral-ε-*H* × 2), 7.02 (2H, dd, $J = 3.2$, 8.4 Hz, Tyral-δ-*H* × 2), 7.27 (1H, d, $J = 8.0$ Hz, naphthyl-*H*), 7.41 (1H, t, $J = 8.0$ Hz, naphthyl-*H*), 7.49 (2H, m, naphthyl-*H*$_2$), 7.81 (2H, d, $J = 8.0$ Hz, naphthyl-*H*$_2$), 7.87 (1H, d, $J = 8.0$ Hz, naphthyl-*H*). ^{13}C-NMR (100 MHz, $CDCl_3/CD_3OD$) δ: 18.0 (*C*H$_3$), 19.2 (*C*H$_3$), 31.1 (Val-β-*C*H), 34.8 (Tyral-β-*C*H$_2$), 36.9 (Tyr-β-*C*H$_2$), 40.9 (*C*H$_2$CO), 55.0 (Tyral-α-*C*H), 55.7 (Tyr-α-*C*H), 59.6 (Val-α-*C*H), 97.7 (hemiacetal-*C*), 115.6 (Tyr-ε-*C*H), 115.7 (Tyral-ε-*C*H), 123.9 (naphthyl-*C*H), 126.0 (naphthyl-*C*H), 126.4 (naphthyl-*C*H), 127.1 (naphthyl-*C*H), 127.4 (Tyr-γ-*C*), 128.5 (naphthyl-*C*H), 128.6 (naphthyl-*C*H), 129.2 (naphthyl-*C*H), 129.3 (Tyral-γ-*C*), 130.4 (Tyr-δ-*C*H), 130.6 (Tyral-δ-*C*H), 131.1 (naphthyl-*C*), 132.5 (naphthyl-*C*), 134.4 (naphthyl-*C*), 155.8 (Tyral-ζ-*C*), 156.1 (Tyr-ζ-*C*), 172.0 (Val-*C*O), 172.6 (Tyr-*C*O), 172.7 (CH$_2$*C*O).

2-Naphthylacetyl-L-tyrosyl-L-valyl-DL-tyrosinal (TP-103). TP-103 was synthesized by a similar procedure to that for TP-104 in a 45% yield from **6**. Mp 176–181 °C. $[\alpha]_D^{26}$ −38.8° (*c* 0.4, MeOH). Rf 0.50 ($CHCl_3$/MeOH = 10/1). APCI-MS *m/z*: 596 $(M+H)^+$, 594 $(M-H)^-$. HRFAB-MS *m/z*: calcd. for $C_{35}H_{38}O_6N_3$, 596.2761; found, 596.2756 $(M+H)^+$. IR (KBr) ν_{max} cm^{-1}: 3280, 2965, 1725, 1640, 1540, 1515, 1230, 825. ^{1}H-NMR (400 MHz, CD_3OD) δ: 0.77 (3H, d, $J = 6.8$ Hz, C*H*$_3$), 0.82 (3H, dd, $J = 2.4$, 6.8 Hz, C*H*$_3$), 1.88–1.95 (1H, m, Val-β-*H*), 2.62 (1H, m, Tyral-β-*H*), 2.76 (1H, ddd, $J = 2.4$, 10.0, 14.0 Hz, Tyr-β-*H*), 2.88 (1H, m, Tyral-β-*H*), 2.98 (1H, dd, $J = 4.4$, 14.0 Hz, Tyr-β-*H*), 3.63 (2H, d, $J = 9.4$ Hz, C*H*$_2$CO), 4.05 (1H, m, Tyral-α-*H*), 4.10 (1H, dd, $J = 2.6$, 7.4 Hz, Val-α-*H*), 4.43 (1H, dd, $J = 4.2$, 6.2 Hz, hemiacetal-*H*), 4.62 (1H, m, Tyr-α-*H*), 6.60 (2H, dd, $J = 2.2$, 8.6 Hz, Tyr-ε-*H* × 2), 6.65 (2H, d, $J = 8.4$ Hz, Tyral-ε-*H* × 2), 6.98 (2H, d, $J = 3.2$, 8.6 Hz, Tyral-δ-*H* × 2), 7.01 (2H, dd, $J = 1.4$, 8.4 Hz, Tyr-δ-*H* × 2), 7.18 (1H, d, $J = 8.4$ Hz, naphthyl-*H*$_2$), 7.41–7.46 (2H, m, naphthyl-*H*$_2$), 7.59 (1H, s, naphthyl-*H*), 7.72 (1H, d, $J = 8.4$ Hz, naphthyl-*H*), 7.74–7.81 (2H, m, naphthyl-*H*$_2$). ^{13}C-NMR (100 MHz, CD_3OD) δ: 18.6 (*C*H$_3$), 19.7 (*C*H$_3$), 32.2 (Val-β-*C*H), 34.9 (Tyral-β-*C*H$_2$), 37.7 (Tyr-β-*C*H$_2$), 43.8 (*C*H$_2$CO), 56.2 (Tyral-α-*C*H), 56.7 (Tyr-α-*C*H), 60.3 (Val-α-*C*H), 98.7 (hemiacetal-*C*), 116.2 (Tyr-ε-*C*H), 116.3 (Tyral-ε-*C*H), 126.8 (naphthyl-*C*H), 127.1 (naphthyl-*C*H), 128.3 (naphthyl-*C*H), 128.6 (naphthyl-*C*H), 128.8 (naphthyl-*C*H), 129.1 (Tyr-γ-*C*), 129.2 (naphthyl-*C*H), 130.3 (naphthyl-*C*H), 130.5 (Tyral-γ-*C*), 131.3 (Tyr-δ-*C*H), 131.4 (Tyral-δ-*C*H), 133.9 (naphthyl-*C*), 134.1 (naphthyl-*C*), 135.0 (naphthyl-*C*), 156.8 (Tyral-ζ-*C*), 157.3 (Tyr-ζ-*C*), 173.1 (Val-*C*O), 173.6 (Tyr-*C*O), 173.9 (CH$_2$*C*O).

Synthesis of the methyl derivatives.

Isovaleryl-(O-benzyl)-L-tyrosyl-L-valyl-(di-O-acetyl)-L-tyrosinol (11). Compound **11** was synthesized by a similar procedure to that for **7** in an 88% yield from **4**. APCI-MS *m/z* 688 $(M+H)^+$. ^{1}H-NMR (400 MHz, $CDCl_3$) δ: 0.75 (3H, d, $J = 6.8$ Hz, C*H*$_3$), 0.85 (3H, d, $J = 6.8$ Hz, C*H*$_3$), 0.86 (3H, d, $J = 6.8$ Hz, C*H*$_3$), 0.87 (3H, d, $J = 6.8$ Hz, C*H*$_3$), 2.02 (2H, d, $J = 2.0$ Hz, $(CH_3)_2CHCH_2CO$), 2.07 (3H, s, COC*H*$_3$), 2.13 (2H, m, Val-β-*H*, $(CH_3)_2CHCH_2CO$), 2.25 (3H, s, COC*H*$_3$), 2.77 (1H, dd, $J = 7.2$, 14.0 Hz, Tyrol-β-*H*), 2.84 (1H, dd, $J = 6.8$, 14.0 Hz, Tyrol-β-*H*), 2.97 (1H, dd, $J = 7.8$, 14.2 Hz, Tyr-β-*H*), 3.05 (1H, dd, $J = 6.2$, 14.2 Hz, Tyr-β-*H*), 4.06 (2H, d, $J = 5.2$ Hz, CHC*H*$_2$O), 4.12 (1H, dd, $J = 6.4$, 8.4 Hz, Val-α-*H*), 4.38 (1H, m, Tyrol-α-*H*), 4.60 (1H, dd, $J = 7.2$, 14.0 Hz, Tyr-α-*H*), 5.00 (2H, s,

OCH_2Ph), 6.01 (1H, d, $J = 7.2$ Hz, N*H*), 6.34 (1H, d, $J = 8.4$ Hz, N*H*), 6.60 (1H, d, $J = 8.8$ Hz, N*H*), 6.90 (2H, d, $J = 8.8$ Hz, Tyr-ε-*H* × 2), 6.98 (2H, d, $J = 8.8$ Hz, Tyrol-ε-*H* × 2), 7.11 (2H, d, $J = 8.8$ Hz, Tyr-δ-*H* × 2), 7.19 (2H, d, $J = 8.8$, Tyr-δ-*H* × 2), 7.30–7.40 (5H, m, Ph-H_5).

Isovaleryl-(O-benzyl)-L-tyrosyl-L-valyl-(O-methyl)-L-tyrosinol (12). Compound **11** was deacetylated by a similar procedure to that for **9**. To a solution of deacetylated **11** (172 mg, 0.28 mmol) in 6 ml of MeOH was added 2 ml of $CHCl_3$, 14.8 mg of *N,N*-diisopropylethylamine (DIEA, 0.11 mmol) and 300 mg of trimethylsilyldiazomethane (2.63 mmol). The reaction mixture was stirred for 24 h at room temperature. The solvent was evaporated to give **12** (294 mg) as a white powder in a quantitative yield from **11**. APCI-MS *m/z*: 618 $(M + H)^+$, 616 $(M + H)^-$. ^{1}H-NMR (400 MHz, CD_3OD) δ: 0.81 (3H, d, $J = 6.4$ Hz, CH_3), 0.85 (3H, d, $J = 6.8$ Hz, CH_3), 0.86 (3H, d, $J = 6.4$ Hz, CH_3), 0.89 (3H, d, $J = 6.8$ Hz, CH_3), 1.97–2.02 (4H, m, Val-β-*H*, $(CH_3)_2CHCH_2CO$), 2.71 (1H, dd, $J = 7.2$, 14.0 Hz, Tyrol-β-*H*), 2.82 (2H, m, Tyrol-β*H*, Tyr-β-*H*), 3.03 (1H, dd, $J = 5.8$, 14.2 Hz, Tyr-β-*H*), 3.49 (2H, m, $CHCH_2O$), 3.72 (3H, s, OCH_3), 4.05 (1H, m, Tyrol-α-*H*), 4.07 (1H, d, $J = 7.2$ Hz, Val-α-*H*), 4.61 (1H, dd, $J = 6.0$, 8.8 Hz, Tyr-α-*H*), 5.00 (2H, s, OCH_3Ph), 6.79 (2H, d, $J = 8.8$ Hz, Tyr-ε-*H* × 2), 6.88 (2H, d, $J = 8.8$ Hz, Tyrol-ε-*H* × 2), 7.12 (2H, d, $J = 8.8$ Hz, Tyr-δ-*H* × 2), 7.14 (2H, d, $J = 8.8$, Tyrol-δ-*H* × 2), 7.30–7.40 (5H, m, Ph-H_5).

Isovaleryl-L-tyrosyl-L-valyl-(O-methyl)-DL-tyrosinal (TP-106). TP-106 was synthesized by a similar procedure to that for **5** and TP-104 in a 38% yield from **12**. Mp 145–147 °C. $[\alpha]_D^{24}$ −32.1° (*c* 0.43, MeOH). Rf 0.50 ($CHCl_3$/MeOH = 10/1). APCI-MS *m/z*: 526 $(M + H)^+$, 524 $(M - H)^-$. HRFAB-MS *m/z*: calcd. for $C_{29}H_{40}O_6N_3$, 526.2917; found, 526.2917 $(M + H)^+$. IR (KBr) ν_{max} cm^{-1}: 3280, 2960, 1735, 1635, 1545, 1515, 1245, 1035, 830. ^{1}H-NMR (400 MHz, CD_3OD) δ: 0.75 (3H, d, $J = 6.4$ Hz, CH_3), 0.81 (3H, d, $J = 6.4$ Hz, CH_3), 0.86 (3H, d, $J = 6.8$ Hz, CH_3), 0.89 (3H, d, $J = 6.8$ Hz, CH_3), 1.90 (1H, m, $(CH_3)_2CHCH_2$), 1.98 (1H, m, Val-β-*H*), 1.99 (2H, d, $J = 6.8$ Hz, CH_2CO), 2.61–2.75 (2H, m, Tyr-β-*H*, Tyral-β-*H*), 2.89–3.05 (2H, m, Tyr-β-*H*, Tyral-β-*H*), 3.65 (3H, s, OCH_3), 4.06–4.14 (2H, m, Tyral-α-*H*, Val-α-*H*), 4.44 (1H, dd, $J = 4.2$, 7.0 Hz, hemiacetal-*H*), 4.59 (1H, m, Tyr-α-*H*), 6.67 (2H, m, Tyr-ε-*H* × 2), 6.77 (2H, d, $J = 8.2$ Hz, Tyral-ε-*H* × 2), 7.04 (2H, m, Tyr-δ-*H* × 2), 7.11 (2H, d, $J = 8.2$ Hz, Tyral-δ-*H* × 2). ^{13}C-NMR (100 MHz, CD_3OD) δ: 17.7 (CH_3), 18.1 (CH_3), 22.3 (CH_3), 22.4 (CH_3), 26.2 $(CH_3)_2CHCH_2$), 30.7 (Val-β-*C*H), 34.3 (Tyral-β-CH_2), 37.1 (Tyr-β-CH_2), 45.6 (CH_2CO), 54.5 (Tyral-α-*C*H), 55.3 (OCH_3), 55.6 (Tyr-α-*C*H), 59.2 (Val-α-*C*H), 96.9 (hemiacetal-*C*), 114.0 (Tyr-ε-*C*H), 115.6 (Tyral-ε-*C*H), 127.4 (Tyr-γ-*C*), 129.8 (Tyral-γ-*C*), 130.0 (Tyr-δ-*C*H), 130.2 (Tyral-δ-*C*H), 155.9 (Tyral-ζ-*C*), 158.3 (Tyr-ζ-*C*), 171.7 (Val-*C*O), 172.8 (Tyr-*C*O), 173.6 (CH_2CO).

(N-t-Butoxycarbonyl-O-benzyl)-L-tyrosyl-L-valyl-(O-methyl)-L-tyrosinol (13). Compound **13** was synthesized by a similar procedure to that for **12** in an 82% yield from **4**. APCI-MS *m/z* 634 $(M + H)^+$. ^{1}H-NMR (400 MHz, $CDCl_3$) δ: 0.75 (3H, d, $J = 6.8$ Hz, CH_3), 0.85 (3H, d, $J = 6.8$ Hz, CH_3), 1.43 (9H, s, $C(CH_3)_3$), 2.23 (1H, m, Val-β-*H*), 2.73 (1H, dd, $J = 6.8$, 13.7 Hz, Tyrol-β-*H*), 2.81 (1H, dd, $J = 8.0$, 13.7 Hz, Tyrol-β-*H*), 2.98 (1H, dd, $J = 7.0$, 14.2 Hz, Tyr-β-*H*), 3.06 (1H, dd, $J = 5.9$, 14.2 Hz, Tyr-β-*H*), 3.50 (1H, dd, $J = 6.1$, 11.2 Hz, $CHCH_2O$), 3.66 (1H, dd, 2.5, 11.2 Hz), 3.76 (3H, s, OCH_3), 4.13 (2H, m, Tyrol-α-*H*, Val-α-*H*), 4.23 (1H, dd, $J = 6.1$, 12.0 Hz, Tyr-α-*H*), 4.93 (1H, d, $J = 4.9$ Hz, N*H*), 5.03 (2H, s, OCH_2Ph), 6.35 (1H, br, N*H*), 6.55 (1H, br, N*H*), 6.80 (2H, d, $J = 8.8$ Hz, Tyr-ε-*H* × 2), 6.93 (2H, d, $J = 8.8$ Hz, Tyrol-ε-*H* × 2), 7.11 (2H, d, $J = 8.8$ Hz, Tyr-δ-*H* × 2), 7.12 (2H, d, $J = 8.8$ Hz, Tyrol-δ-*H* × 2), 7.30–7.40 (5H, m, Ph-H_5).

(N-t-Butoxycarbonyl-O-acetyl)-L-tyrosyl-L-valyl-(O-acetyl-O-methyl)-L-tyrosinol (14). Compound **14** was synthesized by a similar procedure to that for **5** and **6** in a 92% yield from **13**. APCI-MS *m/z* 628 $(M + H)^+$. ^{1}H-NMR (400 MHz, $CDCl_3$) δ: 0.79 (3H, d, $J = 7.2$ Hz, CH_3), 0.86 (3H, d, $J = 7.2$ Hz, CH_3), 1.42 (9H, s, $C(CH_3)_3$), 2.07 (3H, s, $COCH_3$), 2.14 (1H, m, Val-β-*H*), 2.26 (3H, s, $COCH_3$), 2.70 (1H, dd, $J = 8.0$, 14.0 Hz, Tyrol-β-*H*), 2.80 (1H, dd, $J = 6.0$, 14.0 Hz, Tyrol-β-*H*), 3.08 (2H, m, Tyr-β-H_2), 3.77 (3H, s, OCH_3), 4.03 (2H, d, $J = 5.2$ Hz, $CHCH_2O$), 4.13 (1H, m, Val-α-*H*), 4.30 (1H, m, Tyr-α-*H*), 4.38 (1H, m, Tyrol-α-*H*), 4.92 (1H, d, $J = 6.4$ Hz, N*H*), 6.25 (1H, b, N*H*), 6.52 (1H, d, $J = 8.4$ Hz, N*H*), 6.82 (2H, d, $J = 8.6$ Hz, Tyr-ε-*H* × 2), 7.02 (2H, d, $J = 8.6$ Hz, Tyrol-ε-*H* × 2), 7.09 (2H, d, $J = 8.6$ Hz, Tyr-δ-*H* × 2), 7.20 (2H, d, $J = 8.6$ Hz, Tyrol-δ-*H* × 2).

1-Naphthylacetyl-L-tyrosyl-L-valyl-(O-methyl)-DL-tyrosinal (TP-108). TP-108 was synthesized by a similar procedure to that for **7**, **9** and TP-104 in a 64% yield from **14**. Mp 208–210 °C. $[\alpha]_D^{26}$ −27.4° (*c* 0.19, MeOH). Rf 0.47 ($CHCl_3$/MeOH = 10/1). APCI-MS *m/z*: 610 $(M + H)^+$, 608 $(M - H)^-$. HRFAB-MS *m/z*: calcd. for $C_{36}H_{40}O_6N_3$, 610.2917; found, 610.2930 $(M + H)^+$. IR (KBr) ν_{max} cm^{-1}: 3280, 2960, 1730, 1640, 1540, 1510, 1250, 780. ^{1}H-NMR (400 MHz, $CDCl_3/CD_3OD$) δ: 0.75 (3H, dd, $J = 2.4$, 6.8 Hz, CH_3), 0.82 (3H, dd, $J = 2.4$, 6.8 Hz, CH_3), 1.94 (1H, m, Val-β-*H*), 2.64–2.72 (2H, m, Tyr-β-*H*, Tyral-β-*H*), 2.81–2.97 (2H, m, Tyr-β-*H*, Tyral-β-*H*), 3.66 (3H, d, $J = 3.2$ Hz, OCH_3), 3.96 (2H, s, CH_2CO), 4.03 (1H, t, $J = 7.0$ Hz, Tyral-α-*H*), 4.12 (1H, m, Val-α-*H*), 4.44 (1H, dd, $J = 2.4$, 4.0 Hz, hemiacetal-*H*), 4.56 (1H, m, Tyr-α-*H*), 6.57 (2H, dd, $J = 5.6$, 8.6 Hz, Tyr-ε-*H* × 2), 6.76 (4H, m, Tyr-δ-*H* × 2, Tyral-ε-*H* × 2), 7.10 (2H, dd, $J = 2.2$, 8.6 Hz, Tyral-δ-*H* × 2), 7.27 (1H, d, $J = 8.0$ Hz, naphthyl-*H*), 7.40 (1H, t, $J = 8.0$ Hz, naphthyl-*H*), 7.48 (2H, m, naphthyl-H_2), 7.79 (2H, d, $J = 8.0$ Hz, naphthyl-H_2), 7.86 (1H, d, $J = 8.8$ Hz, naphthyl-*H*). ^{13}C-NMR (100 MHz, $CDCl_3/CD_3OD$) δ: 18.2 (CH_3),

19.3 (CH_3), 31.2 (Val-β-CH), 34.8 (Tyral-β-CH_2), 37.2 (Tyr-β-CH_2), 41.2 (CH_2CO), 55.3 (Tyral-α-CH), 55.5 (OCH_3), 55.8 (Tyr-α-CH), 59.8 (Val-α-CH), 98.0 (hemiacetal-C), 114.4 (Tyr-ε-CH), 116.0 (Tyral-ε-CH), 124.1 (naphthyl-CH), 126.1 (naphthyl-CH), 126.5 (naphthyl-CH), 127.2 (naphthyl-CH), 127.7 (Tyr-γ-C), 128.7 (naphthyl-CH), 128.8 (naphthyl-CH), 129.3 (naphthyl-CH), 130.7 (Tyr-δ-CH), 130.8 (Tyral-δ-CH), 130.9 (Tyral-γ-C), 131.4 (naphthyl-C), 132.8 (naphthyl-C), 134.7 (naphthyl-C), 156.4 (Tyral-ζ-C), 158.9 (Tyr-ζ-C), 172.3 (Val-CO), 172.5 (Tyr-CO), 172.8 (CH_2CO).

*(N-t-Butoxycarbonyl-O-methyl)-L-tyrosyl-L-valyl-(di-O-acetyl)-L-tyrosinol (**15**).* Compound **15** was synthesized by a similar procedure to that for **12** in a 40% yield from **5**. APCI-MS m/z 628 $(M+H)^+$. ^{1}H-NMR (400 MHz, $CDCl_3$) δ: 0.76 (3H, d, $J = 7.0$ Hz, CH_3), 0.85 (3H, d, $J = 7.0$ Hz, CH_3), 1.41 (9H, s, $C(CH_3)_3$), 2.07 (3H, m, $COCH_3$), 2.15 (1H, m, Val-β-H), 2.27 (3H, s, $COCH_3$), 2.73–2.85 (2H, m, Tyrol-βH_2), 3.03 (2H, t, $J = 5.8$ Hz, Tyr-β-H_2), 3.76 (3H, s, OCH_3), 4.02 (2H, d, $J = 4.4$ Hz, $CHCH_2O$), 4.13 (2H, dd, 6.6, 7.4 Hz, Val-α-H), 4.24 (1H, dd, $J = 7.4$, 14.0 Hz, Tyr-α-H), 4.41 (1H, m, Tyrol-α-H), 4.90 (1H, br, NH), 6.36 (1H, br, NH), 6.44 (1H, d, $J = 8.4$ Hz, NH), 6.83 (2H, d, $J = 8.6$ Hz, Tyr-ε-$H \times 2$), 7.00 (2H, d, $J = 8.6$ Hz, Tyrol-ε-$H \times 2$), 7.11 (2H, d, $J = 8.6$ Hz, Tyr-δ-$H \times 2$), 7.19 (2H, d, $J = 8.6$ Hz, Tyrol-δ-$H \times 2$).

1-Naphthylacetyl-(O-methyl)-L-tyrosyl-L-valyl-DL-tyrosinal (TP-109). TP-109 was synthesized by a similar procedure to that for TP-108 in a 14% yield from **15**. Mp 150–153 °C. $[\alpha]_D^{23}$ −18.2° (c 0.17, MeOH). Rf 0.45 ($CHCl_3$/MeOH = 10/1). APCI-MS m/z: 610 $(M+H)^+$, 608 $(M-H)^-$. HRFAB-MS m/z: calcd. for $C_{36}H_{40}O_6N_3$, 610.2917; found, 610.2901 $(M+H)^+$. IR (KBr) ν_{max} cm^{-1}: 3270, 2960, 1740, 1640, 1540, 1510, 1250, 780. ^{1}H-NMR (400 MHz, $CDCl_3$/CD_3OD) δ: 0.75 (3H, dd, $J = 4.0$, 6.8 Hz, CH_3), 0.81 (3H, dd, $J = 4.0$, 6.8 Hz, CH_3), 1.95 (1H, m, Val-β-H), 2.60–2.92 (4H, m, Tyr-β-$H \times 2$, Tyral-β-$H \times 2$), 3.73 (3H, d, $J = 4.4$ Hz, OCH_3), 3.97 (2H, s, CH_2CO), 4.02 (1H, m, Tyral-α-H), 4.03–4.08 (1H, br, Val-α-H), 4.41 (1H, d, $J = 4.0$ Hz, hemiacetal-H), 4.59 (1H, m, Tyr-α-H), 6.56 (2H, dd, $J = 8.8$, 10.8 Hz, Tyr-ε-$H \times 2$), 6.72 (4H, m, Tyr-δ-$H \times 2$, Tyral-ε-$H \times 2$), 7.03 (2H, dd, $J = 3.2$, 8.8 Hz, Tyral-δ-$H \times 2$), 7.30 (1H, d, $J = 8.8$ Hz, naphthyl-H), 7.41 (1H, t, $J = 8.8$ Hz, naphthyl-H_2), 7.45–7.53 (2H, m, naphthyl-H_2), 7.81 (2H, d, $J = 8.8$ Hz, naphthyl-H_2), 7.88 (1H, d, $J = 8.8$ Hz, naphthyl-H). ^{13}C-NMR (100 MHz, $CDCl_3$/CD_3OD) δ: 18.0 (CH_3), 19.1 (CH_3), 30.9 (Val-β-CH), 34.8 (Tyral-β-CH_2), 36.8 (Tyr-β-CH_2), 41.0 (CH_2CO), 54.7 (Tyral-α-CH), 55.3 (OCH_3), 55.6 (Tyr-α-CH), 59.3 (Val-α-CH), 97.6 (hemiacetal-C), 114.1 (Tyr-ε-CH), 115.5 (Tyral-ε-CH), 123.8 (naphthyl-CH), 125.9 (naphthyl-CH), 126.3 (naphthyl-CH), 127.0 (naphthyl-CH), 128.2 (Tyr-γ-C), 128.5 (naphthyl-CH), 128.6 (naphthyl-CH), 128.9 (Tyral-γ-C), 129.0 (naphthyl-CH), 130.2 (Tyr-δ-CH), 130.4 (Tyral-δ-CH), 130.8 (naphthyl-C), 132.3 (naphthyl-C), 134.3 (naphthyl-C), 155.6 (Tyral-ζ-C), 158.6 (Tyr-ζ-C), 171.8 (Val-CO), 172.3 (Tyr-CO), 172.4 (CH_2CO).

Isovaleryl-(O-methyl)-L-tyrosyl-L-valyl-(O-methyl)-DL-tyrosinal (TP-107). TP-107 was synthesized by a similar procedure to that for **12** and TP-104 in a 27% yield from tyropeptinol A. Mp 158–161 °C. $[\alpha]_D^{24}$ −28.0° (c 0.25, MeOH). Rf 0.41 ($CHCl_3$/MeOH = 10/1). APCI-MS m/z: 540 $(M+H)^+$, 538 $(M-H)^-$. HRFAB-MS m/z: calcd. for $C_{30}H_{42}O_6N_3$, 540.3074; found, 540.3109 $(M+H)^+$. IR (KBr) ν_{max} cm^{-1}: 3280, 2960, 1730, 1640, 1550, 1510, 1250, 1040. ^{1}H-NMR (400 MHz, $CDCl_3$) δ: 0.79 (3H, m, CH_3), 0.86 (3H, m, CH_3), 0.87 (3H, m, CH_3), 0.88 (3H, d, $J = 6.8$ Hz, CH_3), 2.03 (2H, br, CH_2CO), 2.04 (1H, m, $(CH_3)_2CHCH_2$), 2.13 (1H, m, Val-β-H), 2.78 (1H, m, Tyral-β-H), 2.97–3.06 (3H, m, Tyral-β-H, Tyr-β-$H \times 2$), 3.76 (6H, s, $OCH_3 \times 2$), 4.21 (1H, m, Tyral-α-H), 4.62 (1H, m, Val-α-H), 4.64 (1H, m, Tyr-α-H), 5.99 (1H, br, NH) 6.44 (1H, br, NH), 6.78–6.86 (4H, m, Tyr-ε-$H \times 2$, Tyral-ε-$H \times 2$), 7.06–7.18 (4H, m, Tyr-δ-$H \times 2$, Tyral-δ-$H \times 2$), 9.56 (1H, s, CHO). ^{13}C-NMR (100 MHz, $CDCl_3$) δ: 17.5 (CH_3), 19.1 (CH_3), 22.3 (CH_3), 22.4 (CH_3), 26.1 $(CH_3)_2$-$CHCH_2$), 30.3 (Val-β-CH), 34.2 (Tyral-β-CH_2), 36.8 (Tyr-β-CH_2), 45.8 (CH_2CO), 54.6 (Tyral-α-CH), 55.3 (OCH_3), 55.4 (OCH_3), 58.6 (Tyr-α-CH), 59.8 (Val-α-CH), 114.2 (Tyr-ε-CH), 114.3 (Tyral-ε-CH), 127.5 (Tyr-γ-C), 128.2 (Tyral-γ-C), 130.2 (Tyr-δ-CH), 130.3 (Tyral-δ-CH), 158.7 (Tyral-ζ-C), 158.8 (Tyr-ζ-C), 170.7 (Val-CO), 171.3 (Tyr-CO), 173.0 (CH_2CO), 198.9 (CHO).

1-Naphthylacetyl-(O-methyl)-L-tyrosyl-L-valyl-(O-methyl)-DL-tyrosinal (TP-110). TP-110 was synthesized by a similar procedure to that for TP-107 in a 52% yield from **9**. Mp 192–194 °C. $[\alpha]_D^{28}$ −12.0° (c 0.25, DMF). Rf 0.62 ($CHCl_3$/MeOH = 10/1). APCI-MS m/z: 624 $(M+H)^+$, 622 $(M-H)^-$. HRFAB-MS m/z: calcd. for $C_{37}H_{42}O_6N_3$, 624.3074; found, 624.3065 $(M+H)^+$. IR (KBr) ν_{max} cm^{-1}: 3280, 2960, 1730, 1640, 1540, 1510, 1250, 1040, 780. ^{1}H-NMR (400 MHz, $CDCl_3$/CD_3OD) δ: 0.76 (3H, dd, $J = 4.8$, 6.0 Hz, CH_3), 0.82 (3H, dd, $J = 4.8$, 6.0 Hz, CH_3), 1.95 (1H, m, Val-β-H), 2.66–2.73 (2H, m, Tyr-β-H, Tyral-β-H), 2.80–2.96 (2H, m, Tyr-β-H, Tyral-β-H), 3.68 (3H, d, $J = 5.2$ Hz, OCH_3), 3.74 (3H, d, $J = 4.0$ Hz, OCH_3), 3.96 (2H, s, CH_2CO), 4.00 (1H, t, $J = 7.6$ Hz, Val-α-H), 4.03–4.18 (1H, m, Tyral-α-H), 4.42 (1H, d, $J = 4.0$ Hz, hemiacetal-H), 4.58 (1H, m, Tyr-α-H), 6.58 (2H, t, $J = 8.8$ Hz, Tyr-ε-$H \times 2$), 6.76 (4H, dd, $J = 2.0$, 8.8 Hz, Tyr-δ-$H \times 2$, Tyral-ε-$H \times 2$), 7.20 (2H, dd, $J = 3.2$, 8.8 Hz, Tyral-δ-$H \times 2$), 7.30 (1H, d, $J = 8.4$ Hz, naphthyl-H), 7.41 (1H, t, $J = 8.4$ Hz, naphthyl-H), 7.45–7.52 (2H, m, naphthyl-H_2), 7.81 (2H, d, $J = 8.4$ Hz, naphthyl-H_2), 7.88 (1H, d, $J = 8.4$ Hz, naphthyl-H). ^{13}C-NMR (100 MHz, $CDCl_3$/CD_3OD) δ: 18.1 (CH_3), 19.2 (CH_3), 30.9 (Val-β-CH), 34.7 (Tyral-β-CH_2), 36.9 (Tyr-β-CH_2), 41.2 (CH_2CO), 54.7 (Tyr-α-CH), 55.3 (OCH_3), 55.4 (OCH_3), 55.5 (Tyr-α-CH), 59.6 (Val-α-CH), 97.6 (hemiacetal-C), 114.1 (Tyr-ε-CH), 114.2 (Tyral-ε-CH), 123.9 (naphthyl-CH),

125.9 (naphthyl-*C*H), 126.3 (naphthyl-*C*H), 127.0 (naphthyl-*C*H), 128.4 (Tyr-γ-*C*), 128.5 (naphthyl-*C*H), 128.6 (naphthyl-*C*H), 129.1 (naphthyl-*C*H), 130.3 (Tyr-δ-*C*H), 130.4 (Tyral-γ-*C*), 130.5 (Tyral-δ-*C*H), 131.0 (naphthyl-*C*), 132.4 (naphthyl-*C*), 134.4 (naphthyl-*C*), 158.5 (Tyral-ζ-*C*), 158.7 (Tyr-ζ-*C*), 171.9 (Val-*C*O), 172.4 (Tyr-*C*O), 172.5 (CH_2*C*O).

Proteasome and α-chymotrypsin activity. The chymotrypsin-like, trypsin-like and PGPH activities of the 20S proteasome and α-chymotrypsin were measured by using fluorogenic substrates as previously described.[9] The 20S proteasome was prepared from human leukemia HL-60 cells.

Cells. RKO human colon carcinoma, SW-480 human colon adenocarcinoma, HT-1080 human fibrosarcoma and RPMI8226 multiple myeloma were obtained from ATCC Cell Bank. RKO and HT-1080 cells were grown in an RPMI1640 medium, RPMI8226 cells were grown in an RPMI1640 medium containing 5.5 μM 2-mercaptoethanol, 1 mM sodium pyruvate and a 0.1 mM MEM non-essential amino acid solution (Invitrogen, Grand island, NY, U.S.A.), and SW-480 cells were grown in an L-15 medium supplemented with 10% fetal bovine serum (Tissue Culture Biologicals, Tulare, CA, U.S.A.), 100 U/ml of penicillin G, and 100 μg/ml of streptomycin at 37 °C with 5% CO_2.

Cell growth. The cells were incubated in 96-well plates at 5,000 cells/well with a test sample for 72 hours. Cell growth was determined by the MTT (3-(4,5-dimethyl-2-thiazolyl)-2,5-diphenyl-2H-tetrazolium bromide) method.

Acknowledgments

We thank Dr. R. Sawa and Ms. Y. Kubota of Microbial Chemistry Research Center for spectroscopic analysis, and Dr. T. Watanabe and Mr. M. Abe of Microbial Chemistry Research Center for useful discussions. This work was supported by the Public Trust Haraguchi Memorial Cancer Research Fund and by grant-aid for scientific research (No. 15790059) from the Japanese Ministry of Education, Culture, Sports, Science and Technology.

References

1) Coux, O., Tanaka, K., and Goldberg, A. L., Structure and functions of the 20S and 26S proteasomes. *Annu. Rev. Biochem.*, **65**, 801–847 (1996).
2) Voges, D., Zwickl, P., and Baumeister, W., The 26S proteasome: A molecular machine designed for controlled proteolysis. *Annu. Rev. Biochem.*, **68**, 1015–1068 (1999).
3) Maki, C. G., and Howley, P. N., Ubiquitination of p53 and p21 is differentially affected by ionizing and UV radiation. *Mol. Cell. Biol.*, **17**, 355–363 (1997).
4) Pagano, M., Tam, S. W., Theodoras, A. M., Beer-Romero, P., Del Sal, G., Chau, V., Yew, P. R., Draetta, G. F., and Rolfe, M., Role of the ubiquitin-proteasome pathway in regulating abundance of the cyclin-dependent kinase inhibitor p27. *Science*, **269**, 682–685 (1995).
5) Ciechanover, A., DiGiuseppe, J. A., Bercovich, B., Orian, A., Richter, J. D., Schwartz, A. L., and Brodeur, G. M., Degradation of nuclear oncoproteins by the ubiquitin system *in vitro*. *Proc. Natl. Acad. Sci. U.S.A.*, **88**, 139–143 (1991).
6) Palombella, V. J., Rando, O. J., Goldberg, A. L., and Maniatis, T., The ubiquitin-proteasome pathway is required for processing the NF-κB1 precursor protein and the activation of NF-κB. *Cell*, **78**, 773–785 (1994).
7) Adams, J., Behnke, M., Chen, S., Cruickshank, A. A., Dick, L. R., Grenier, L., Klunder, J. M., Ma, Y.-T., Plamonda, L., and Stein, R. L., Potent and selective inhibitors of the proteasome: Dipeptidyl boronic acid. *Bioorg. Med. Chem. Lett.*, **8**, 333–338 (1998).
8) Adams, J., Palombella, V. J., Sausville, E. A., Johnson, J., Destree, A., Lazarus, D. D., Maas, J., Pien, C. S., Prakash, S., and Elliott, P. J., Proteasome inhibitors: A novel class of potent and effective antitumor agents. *Cancer Res.*, **59**, 2615–2622 (1999).
9) Momose, I., Sekizawa, R., Hashizume, H., Kinoshita, N., Homma, Y., Hamada, M., Iinuma, H., and Takeuchi, T., Tyropeptins A and B, new proteasome inhibitors produced by *Kitasatospora* sp. MK993-dF2. I. Taxonomy, isolation, physico-chemical properties and biological activities. *J. Antibiotics*, **54**, 997–1003 (2001).
10) Momose, I., Sekizawa, R., Hirosawa, S., Ikeda, D., Naganawa, H., Iinuma, H., and Takeuchi, T., Tyropeptins A and B, new proteasome inhibitors produced by *Kitasatospora* sp. MK993-dF2. II. Structure determination and synthesis. *J. Antibiotics*, **54**, 1004–1012 (2001).
11) Momose, I., Sekizawa, R., Iinuma, H., and Takeuchi, T., Inhibition of proteasome activity by tyropeptin A in PC12 cells. *Biosci. Biotechnol. Biochem.*, **66**, 2256–2258 (2002).
12) Momose, I., Umezawa, Y., Hirosawa, S., Iinuma, H., and Ikeda, D., Structure-based design of derivatives of tyropeptin A as the potent and selective inhibitors of mammalian 20S proteasome. *Bioorg. Med. Chem. Lett.*, **15**, 1867–1871 (2005).
13) Tsubuki, S., Kawasaki, H., Saito, Y., Miyashita, N., Inomata, M., and Kawashima, S., Purification and characterization of a Z-Leu-Leu-Leu-MCA degrading protease expected to regulate neurite formation: a novel catalytic activity in proteasome. *Biochem. Biophys. Res. Commun.*, **196**, 1195–1201 (1993).

Available online at www.sciencedirect.com
SCIENCE DIRECT®
Biochimica et Biophysica Acta 1722 (2005) 247–253
BIOCHIMICA ET BIOPHYSICA ACTA
BBA
http://www.elsevier.com/locate/bba

Regular paper

Apolipoprotein E3 (apoE3) safeguards pig proximal tubular LLC-PK$_1$ cells against reduction in SGLT1 activity induced by gentamicin C

Kozo Takamoto[a], Manabu Kawada[a], Daishiro Ikeda[a,*], Motonobu Yoshida[b]

[a]*Numazu Bio-Medical Research Institute, Microbial Chemistry Research Center, 18-24 Miyamoto, Numazu-shi, Shizuoka 410-0301, Japan*
[b]*Department of Agriculture, Kinki University, 3327-204 Nakamachi, Nara 631-8505, Japan*

Received 27 June 2004; received in revised form 27 October 2004; accepted 2 December 2004
Available online 1 February 2005

Abstract

Megalin, a family of endocytic receptors related to the low-density lipoprotein (LDL) receptor, is a major pathway for proximal tubular aminoglycoside accumulation. We previously reported that aminoglycoside antibiotics reduce SGLT1-dependent glucose transport in pig proximal tubular epithelial LLC-PK$_1$ cells in parallel with the order of their nephrotoxicity. In this study, using a model of gentamicin C (GMC)-induced reduction in SGLT1 activity, we examined whether ligands for megalin protect LLC-PK$_1$ cells from the GMC-induced reduction in SGLT1 activity. We employed apolipoprotein E3 (apoE3) and lactoferrin as ligands for megalin. Then the cells were treated with various concentrations of apoE3, lactoferrin and bovine serum albumin with or without 100 μg/ml of GMC, and the SGLT1-dependent methyl α-D-glucopyranoside (AMG) uptake and levels of SGLT1 expression were determined. As a result, we demonstrated that the apoE3 significantly protects these cells from GMC-induced reduction in AMG uptake, but neither lactoferrin nor albumin does. In accord with a rise in AMG uptake activity, the mRNA and protein levels of SGLT1 were apparently up-regulated in the presence of apoE3. Furthermore, we found that the uptake of [^{3}H] gentamicin is decreased by apoE3, and that apoE3 showed obvious protection against the GMC-dependent *N*-acetyl-β-D-glucosamidase (NAG) release from LLC-PK$_1$ cells. Thus, these results indicate that apoE3 could be a valuable tool for the prevention of aminoglycoside nephrotoxicity.

Keywords: Apolipoprotein E3; SGLT1; Nephrotoxicity; LLC-PK$_1$ cell; *N*-acetyl-β-D-glucosamidase

1. Introduction

Aminoglycosides are commonly used antibiotics for the treatment of serious infections caused by various bacteria including methicillin-resistant *Staphylococcus aureus* (MRSA), while aminoglycosides often cause damage to proximal tubular cells as a consequence of their nephrotoxicity.

As it has been considered that the accumulation of aminoglycosides in proximal tubular epithelial cells leads to membrane structural disturbance and cell death, previous studies had focused on the pathway of aminoglycoside uptake in proximal tubular apical membranes [1,2]. Recently, megalin has been implicated as a main route of renal aminoglycosides uptake [1,3]. Megalin is a large glycoprotein (about 600 kDa) to function as a multi-ligand endocytic receptor related to the low-density lipoprotein (LDL) receptor [1,3], and is expressed on apical surface in proximal tubular cells, ependyma, lung alveoli, and yolk sac [4]. The main function of megalin has been indicated as a pathway for clearance of low molecular weight plasma proteins, which are filtered from glomerulus [4–6]. Furthermore, megalin mediates the uptake of apolipoprotein E3 (apoE3), a 34-kDa glycoprotein, which is the most common isoform of apolipoprotein E (apoE) [4,7]. Recent study has implicated that the primary function of apoE is a lipid transport and promotion of cholesterol efflux from cells [8].

* Corresponding author. Tel.: +81 55 924 0601; fax: +81 55 922 6888.
E-mail address: numazu@bikaken.or.jp (D. Ikeda).

0304-4165/$ - see front matter © 2004 Elsevier B.V. All rights reserved.
doi:10.1016/j.bbagen.2004.12.006

Kounnas et al. found that human milk protein known as apolipoprotein J (apoJ) is a novel megalin ligand, and demonstrated that several ligands for megalin block the binding of apoJ to the receptor. In addition, they suggested that apoJ, apoE3 and lipoprotein lipase carboxyl-terminal receptor binding fragment might share a common binding site on megalin, while other ligand such as lactoferrin presumably binds to away from the site of the receptor [9]. Therefore, if megalin is a main route of aminoglycosides uptake as mentioned above, there is a possibility that ligands for megalin sharing the same binding site might prevent the aminoglycoside nephrotoxicity.

We previously reported that nephrotoxic aminoglycosides significantly reduce Na^+/glucose cotransporter (SGLT1)-dependent glucose transport and down-regulate mRNA and protein levels of the SGLT1 in pig proximal tubular LLC-PK_1 cells [10]. We further demonstrated that the mRNA expression of SGLT1 was down-regulated in the gentamicin C (GMC)-treated murine kidney as well as in vitro, and that was associated with the increase in urinary glucose excretion in GMC-treated mice [10]. Here we employed some ligands for megalin to study whether these proteins protect LLC-PK_1 cells from GMC-induced reduction in SGLT1 activity.

2. Materials and methods

2.1. Materials and cell culture

Methyl α-D-[^{14}C] glucopyranoside (AMG) was purchased from Moravek Biochemicals (Brea, CA). [^{3}H] gentamicin sulfate was from American Radiolabeled Chemicals, Inc. (St. Louis, MO). Human recombinant apoE2, apoE3 and apoE4 were from CALBIOCHEM (San Diego, CA). Lactoferrin from human milk and bovine serum albumin-fraction V were obtained from Sigma (St. Louis, MO). A rabbit polyclonal antibody specific for a porcine SGLT1 was kindly provided by Prof. Julia E. Lever (University of Texas Medical School, Houston). This antibody reacts with a 75-kDa porcine SGLT1 subunit [10]. A mouse anti-β-actin monoclonal antibody (AC-74) was obtained from Sigma (St. Louis, MO). An anti-rabbit Ig horseradish peroxidase-linked whole antibody and an anti-mouse Ig horseradish peroxidase-linked whole antibody were purchased from Amersham Biosciences (Piscataway, NJ). GMC was prepared by us. LLC-PK_1 derived from porcine proximal tubular cells were obtained from American Type Culture Collection (Manassas, VA), and the cells were maintained in a Dulbecco's modified Eagle's medium (DMEM; Nissui Pharmaceutical, Japan) supplemented with 10% fetal bovine serum (FBS) at 37 °C in a 5% CO_2–95% air atmosphere without addition of antibiotics.

2.2. AMG uptake study

Cells were inoculated into 24-well plates at 1×10^5 cells/ml (1 ml/well) with various concentrations of GMC with or without various concentrations of apoE2, apoE3, apoE4, lactoferrin and albumin, and incubated in DMEM supplemented with 10% FBS at 37 °C for 4 days. ^{14}C-labeled AMG (0.4 μCi/ml) was added and after the incubation at 37 °C for 30 min, the medium was immediately removed and the cells were washed twice with ice-cold PBS. The cells were lysed in 0.5 ml of 0.1 N NaOH and 0.1% SDS, and the aliquots of the lysates were employed for the determination of radioactivity and protein concentration. Protein concentration was measured using a protein assay kit (Bio-Rad, Hercules, CA).

2.3. Detection of SGLT1 mRNA expression in LLC-PK_1 cells

Cells (1×10^5 cells/ml) were cultured in 10% FBS DMEM with 0–100 μg/ml of GMC, with or without 4.3 μg/ml of apoE3, 10 μg/ml of lactoferrin and albumin, and the total RNAs were isolated at day 4 as previously described [10]. Subsequently, the RNA extracts were employed for synthesis of cDNA. The primer sets were designed from the GenBank database and the following primers were used for RT-PCR: pig-SGLT1, sense, 5′-TGG ACG AAG TAT GGT GTG GT-3′, and anti-sense, 5′-CAT CAC TAT GAC AAA CAT GG-3′; pig-GAPDH, sense, 5′-GAT GAC ATC AAG AAG GTG GTG AA-3′, and anti-sense, 5′-CTC TTA CTC CTT GGA GGC CAT GT-3′. The conditions for amplification were as follows: 94 °C for 2 min followed by 25 cycles of 94 °C for 30 s, 56 °C for 30 s, and 72 °C for 1 min in a TAKARA PCR Thermal Cycler MP (Takara Bio, Japan). The expression levels of SGLT1 were quantified by Fluoro Image Analyzer FLA-5000 (Fuji Photo Film, Japan).

2.4. Protein preparation from LLC-PK_1 cells and immunoblotting

Cells (1×10^5 cells/ml) were plated onto 24-well plates with 0–200 μg/ml of GMC with or without 4.3 μg/ml of each of three apoE isoforms, 10 μg/ml of lactoferrin and albumin, and cultured in 10% FBS DMEM for 4 days. The cells were washed twice with ice-cold PBS and then lysed in a lysis buffer (20 mM Hepes, pH 7.5, 150 mM NaCl, 1% Triton X-100, 10% glycerol, 1 mM EDTA, 50 mM NaF, 50 mM β-glycerophosphate, 1 mM Na_3VO_4, and 25 μg/ml each of antipain, leupeptin, and pepstatin). The cell lysates were collected and centrifuged at $15{,}000\times g$ for 10 min. The supernatants were retrieved and stocked at −20 °C until just before use.

Equal amounts of protein extracts (approximately 10 μg) were electrophoretically separated by 7.5% SDS-polyacrylamide gel and transferred onto Immobilon polyvinylidine difluoride membranes (Millipore) as previously described [10]. Thereafter, the membrane was incubated

with appropriate antibodies and the membrane was developed by enhanced chemiluminescence system (Amersham Bioscience).

2.5. GMC uptake study

Cells (1×10^5 cells/ml) were inoculated into 24-well plates as described above. After 1 day or 4 days culture, [^{3}H] gentamicin (1 μCi/ml) was added and incubated at 37 °C for 10–120 min with or without 4.3 μg/ml of apoE3 and 100 μg/ml of unlabeled GMC. The cells were washed twice with 0.5 ml of ice-cold PBS, and then cells were lysed in 0.5 ml of 0.1 N NaOH and 0.1% SDS. The radioactivities and protein concentrations were determined as previously described [10].

2.6. Detection of NAG levels

Cells (1×10^5 cells/ml) were inoculated into a 24-well plate with 0–100 μg/ml of GMC, with or without 4.3 μg/ml of apoE3, 10 μg/ml of lactoferrin and albumin, and cultured in 10% FBS DMEM for 4 days. Thereafter, the respective supernatants of the medium were retrieved for a measurement of *N*-acetyl-β-D-glucosamidase (NAG) activity. NAG levels were detected by NAG-TEST SHIONOGI according to manufacture's instructions (Shionogi and Co., Ltd., Japan).

2.7. Statistical analysis

After the results were obtained, sets of data were assigned to their respective groups. The significance of the differences between the sets of data was assessed by Student's *t*-test.

3. Results

3.1. Assessment of GMC-induced reduction in SGLT1 activity

Previously, we demonstrated that nephrotoxic aminoglycosides decrease the glucose transport specifically from apical to basolateral side in LLC-PK$_1$ cells, and that the reduction of AMG uptake was SGLT1-dependent. In our in vitro model, treatment of the cells with 100 μg/ml of GMC or neomycin for 4 days exhibited a striking reduction in the AMG uptake [10]. To establish an appropriate model of GMC-induced reduction in SGLT1 activity, LLC-PK$_1$ cells were cultured with various concentrations of GMC, and then assessed AMG uptake as a specific indicator of SGLT1 activity. As shown in Fig. 1A, GMC reduced the AMG uptake dose-dependently and 100 μg/ml of GMC inhibited it completely. Furthermore, we detected the protein expression levels of SGLT1 and found that GMC decreases the protein level of SGLT1 in agreement with AMG uptake (Fig. 1B).

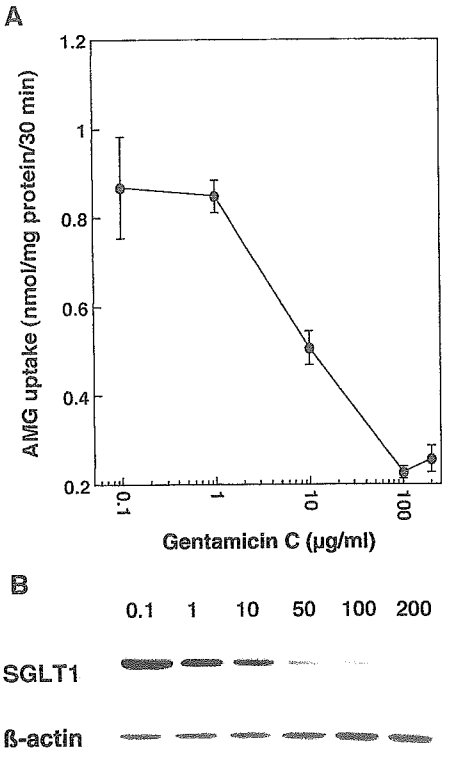

Fig. 1. GMC-induced reduction in SGLT1 activity in LLC-PK$_1$ cells. (A) Cells were cultured for 4 days with various concentrations of GMC, and then 0.4 μCi/ml AMG was added for AMG uptake study. Cells were disrupted and the aliquots were employed for the determination of radioactivity and protein concentrations. (B) Cells were cultured for 4 days, and then total protein extracts were separated by SDS-PAGE and applied to immunoblotting. Membrane was incubated with a rabbit anti-porcine SGLT1 polyclonal antibody and approximately 75-kDa bands were detected. Anti-β-actin monoclonal antibody (42 kDa) was used as an internal control.

Hence, we employed a concentration of 100 μg/ml of GMC for following studies as a nephrotoxic model.

3.2. Protective effect of apoE3 on reduction in SGLT1 activity

In order to investigate the protective effect of apoE3 or lactoferrin which is considered to be a ligand for megalin on GMC-induced reduction in SGLT1 activity, the cells were inoculated with various concentrations of apoE3, lactoferrin and bovine serum albumin with or without GMC and cultured for 4 days. As shown in Fig. 2A, control without any addition displayed high AMG uptake (1.636±0.133 nmol/mg protein/30 min) and other simple addition of the megalin ligands retained the uptake as well as control. While the addition of 100 μg/ml of GMC strongly suppressed the AMG uptake (0.438±0.043 nmol/mg protein/30 min), the addition of 4.3 and 2.15 μg/ml of apoE3 together with GMC significantly improved the uptake (1.249±0.054 and 0.718±0.083 nmol/mg protein/30 min, respectively) and the intensities of the protection were dependent on the dose of apoE3 (Fig 2A). By contrast,

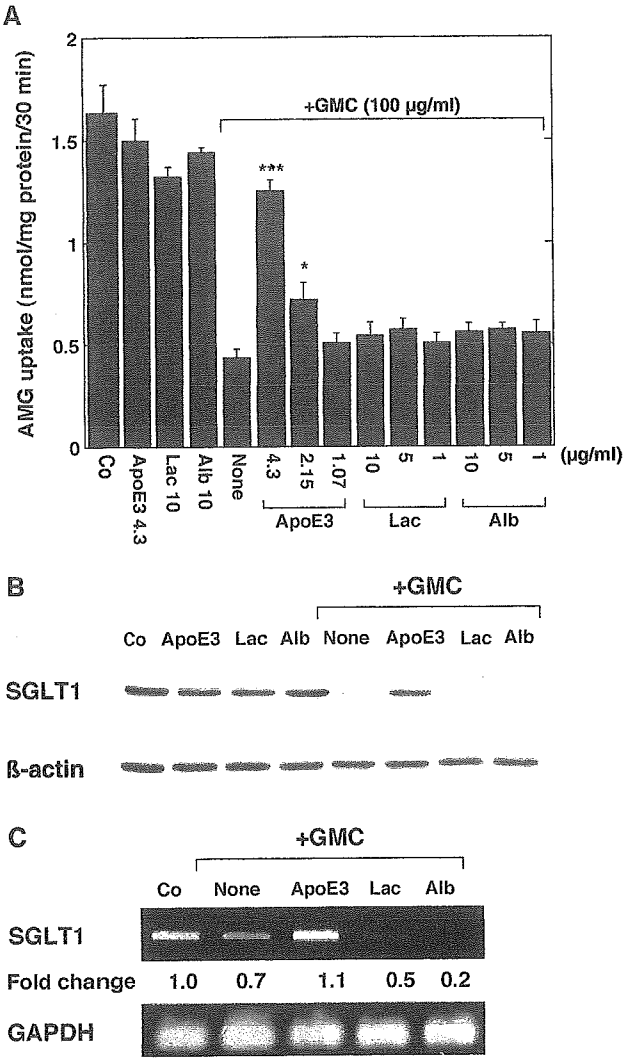

Fig. 2. Effect of ligands for megalin on AMG uptake in LLC-PK$_1$ cells. (A) Cells were cultured with various concentrations of the ligands with or without 100 μg/ml of GMC, and AMG uptake study was carried out as described in Fig. 1. Data represent a mean±S.E. from three independent experiments. *P<0.05; ***P<0.005 versus gentamicin C alone treated group. (B) Western blot analysis was carried out and protein expression levels of SGLT1 were determined as described in Fig. 1. (C) Cells were cultured as described above, and total RNAs were collected at day 4. The amounts of used mRNAs were adjusted to be equally using GAPDH as control. RT-PCR products of SGLT1 and GAPDH were 758 and 236 bp, respectively. Numbers are relative amount of SGLT1 to GAPDH and expressing control as 1.0. Co, control; Lac, lactoferrin; Alb, albumin; and GMC, gentamicin C.

lactoferrin, which may bind to different site of the receptor from the site for apoE3 and albumin did not show any increment in the uptake. Consistent with a rise in AMG uptake activity, the protein and mRNA levels of SGLT1 were apparently up-regulated in the presence of 4.3 μg/ml of apoE3 (Fig. 2B and C). Furthermore, to confirm that common three isoforms of apoE can restore the GMC-induced reduction in AMG uptake, the cells were incubated with 4.3 μg/ml of apoE2, apoE3 and apoE4 with or without GMC. As a result, not only did apoE3 improve the reduction in AMG uptake as described above, but also the addition of apoE2 and apoE4 showed significant increments in AMG uptake and in SGLT1 protein expression (Fig. 3). Because apoE3 is the most prevalent isoforms of apoE, we employed the apoE3 for following studies.

3.3. Effect of apoE3 on [^{3}H] gentamicin uptake

Since the addition of apoE3 protected the cells from GMC-induced reduction in SGLT1 activity, the protective effect is hypothesized to be a result from the interruption of GMC binding and subsequent uptake into the cell. To ascertain whether apoE3 disturbs the binding of GMC to the cell surface as a consequence of inhibition with GMC for binding to the site of the receptor, the cells were inoculated and cultured for 1 or 4 days, and then [^{3}H] gentamicin (1 μCi/ml) was added with or without apoE3 or unlabeled GMC. As shown in Fig. 4, [^{3}H] gentamicin was time-dependently transported into the cells as reported by Kiyomiya et al. [11]. Not merely the addition of 100 μg/ml of unlabeled GMC significantly decreased the uptake of

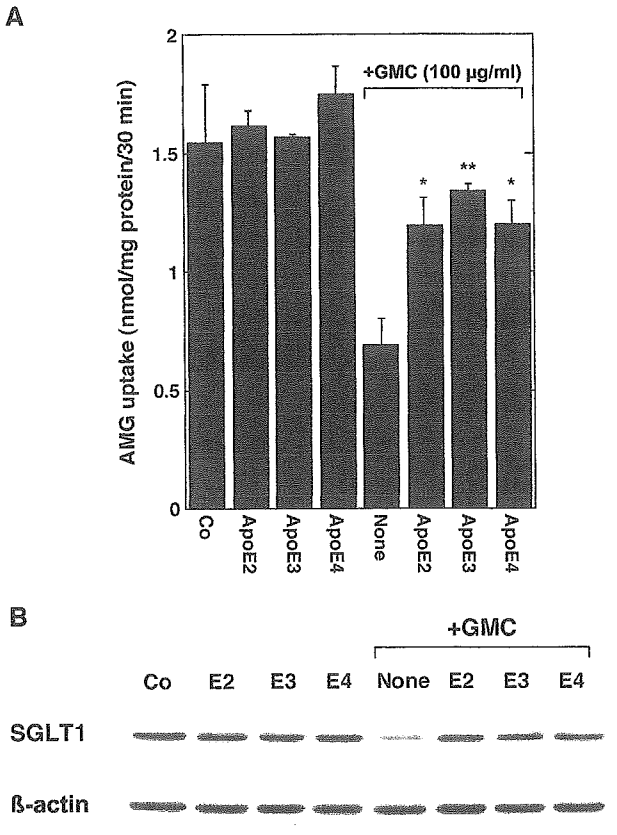

Fig. 3. Effect of three isoforms of apoE on AMG uptake in LLC-PK$_1$ cells. (A) Cells were cultured with 4.3 μg/ml of apoE2, apoE3 and apoE4 with or without 100 μg/ml of GMC, and AMG uptake study was carried out as described in Fig. 1. Data represent a mean±S.E. from three independent experiments. *P<0.05; **P<0.01 versus gentamicin C alone treated group. (B) Western blot analysis was carried out and protein expression levels of SGLT1 were determined as described in Fig. 1. Co, control; E2, apolipoprotein E2; E3, apolipoprotein E3; and E4, apolipoprotein E4.

[^{3}H] gentamicin as observed in vivo [1], but the addition of 4.3 μg/ml of apoE3 showed the interruption of [^{3}H] gentamicin uptake both in subconfluent culture at day one and in confluent culture at day 4. The result indicates that apoE3 disturbs the [^{3}H] gentamicin uptake into the cell.

3.4. Improvement of extracellular release of NAG

Several studies have demonstrated that aminoglycosides localize to lysosomes through endocytic incorporation leading to eventual lysosomal and apical membrane enzymes release [1,12], and that apoE has also shown to be involved in lysosomal localization of high-density lipoprotein (HDL) in a rat kidney [13]. Because we found influence of apoE3 on binding or subsequent uptake of [^{3}H] gentamicin, we postulated that the apoE3 might moderate lysosomal destabilization, which is induced by GMC following intracellular incorporation. To study whether apoE3 improves GMC-dependent extracellular release of NAG, the cells were inoculated and incubated as described above. Thereafter, the release of NAG from the cells into the culture medium was determined. As expected, the GMC-treated cells increased NAG release compared with control cells, and the treatment of cells with 4.3 μg/ml of apoE3 resulted in significant protection against GMC-dependent extracellular NAG release (Fig. 5).

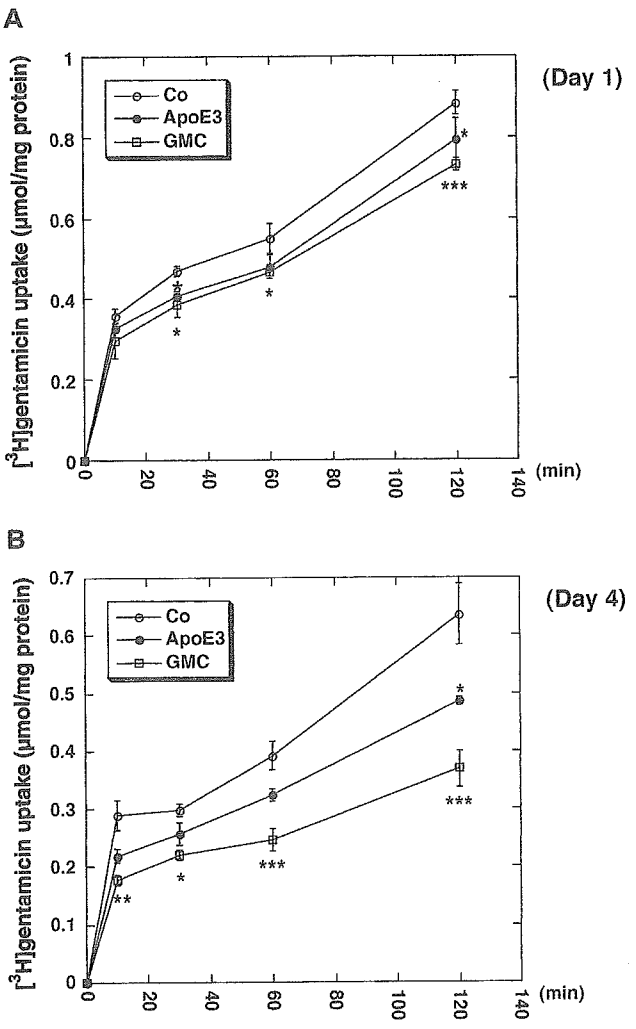

Fig. 4. Effect of apoE3 on [^{3}H] gentamicin uptake in LLC-PK$_1$ cells. Cells were inoculated and cultured for 1 day (A) and for 4 days (B), and 1 μCi/ml of [^{3}H] gentamicin was added and incubated for 10–120 min with or without 4.3 μg/ml of apoE3 or 100 μg/ml of unlabeled GMC. Subsequently, the radioactivities and protein concentrations were determined. Co, [^{3}H] gentamicin alone; and GMC, unlabeled gentamicin. (C) Data represent a mean±S.E. from three independent experiments. *P<0.05; **P<0.01; ***P<0.005 versus control group.

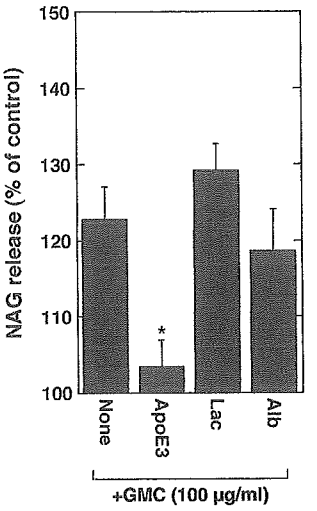

Fig. 5. Effect of apoE3 on the extracellular release of NAG in LLC-PK$_1$ cells. Cells were cultured for 4 days with 0–100 μg/ml of GMC, with or without 4.3 μg/ml of apoE3, 10 μg/ml of lactoferrin and albumin. And then respective supernatants of the medium were retrieved for measurement of NAG activity. Data represent a mean±S.E. from three independent experiments. *P<0.05 versus gentamicin C alone treated group.

4. Discussion

Aminoglycosides are worth using antibiotics for the treatment of severe bacterial infections such as MRSA. Since aminoglycosides accumulate in renal proximal tubular cells and cause subsequent cell death as a result of nephrotoxicity, therapeutic monitoring is essential for the clinical treatment of aminoglycosides. Recent studies demonstrated that megalin is a main route of aminoglycoside uptake in renal proximal tubular cells, and also displayed the evidence that the lack of aminoglycoside uptake is a direct consequence of megalin deficiency in an animal model [1]. Hence, we have postulated that the ligand for megalin might competitively inhibit or interfere the binding of aminoglycosides to the site of the receptor, if they share a common or proximate binding domain.

Our previous study demonstrated that aminoglycosides significantly reduce SGLT1-dependent glucose transport and uptake of AMG, a specific substrate of SGLT1, in LLC-PK$_1$ cells [10]. In this study, we first established an

appropriate model of GMC-induced reduction in SGLT1 activity to examine whether the AMG uptake study reflects the assessment of GMC-dependent nephrotoxicity compared with commonly used nephrotoxic indicator such as LDH release (Fig. 1). Consequently, GMC dose-dependently reduced SGLT1 activity and the result demonstrated the inverse correlation with LDH leakage as reported by Girton et al. [14,15]. This result also showed positive correlation with reduction in Na^+-dependent AMG and phosphate transport in rabbit proximal tubular cells [15] and with inhibitory activity of dome formation in LLC-PK_1 cells as described previously [2,16]. Therefore, we investigated whether ligands for megalin protect LLC-PK_1 cells from GMC-induced reduction in SGLT1 activity. The protective effect was only observed in an addition of apoE3, while it was not observed when lactoferrin, which may bind to away from the site of apoE3, or albumin was added (Fig. 2). Though albumin constitutes the major plasma protein, megalin indirectly mediates endocytosis of albumin through the binding of albumin to cubilin [17]. Thus, it is considered that the binding of albumin to megalin does not affect the binding of aminoglycosides to the site of the receptor. Furthermore, this improvement was at least not due to the activation of SGLT1, because there was no influence on AMG uptake by only the addition of apoE3 (Fig. 2). In addition to the improvement of reduction in SGLT1 activity, apoE3 could sustain the level of SGLT1 mRNA and protein expression (Fig. 2). These results indicate that apoE3 safeguards LLC-PK_1 cells against GMC-induced reduction in SGLT1 activity through the up-regulation of mRNA and the subsequent rise in protein expression of SGLT1. We further found that common three isoforms of apoE show obvious improvement in GMC-induced reduction in AMG uptake and in SGLT1 protein expression (Fig. 3). Although these isoforms differ in two amino acid residues [8], they might share common binding site on the cells.

Consistent with our result, clusterin had also been demonstrated to protect LLC-PK_1 cells from gentamicin-mediated cytotoxicity [14]. Clusterin synonymous with apoJ and apoE are primarily involved in the transport of lipid and cholesterol in the central nervous system, and it has also been suggested that apoJ may play a similar role in lipid trafficking when apoE function is impaired [18]. Moreover, Kounnas et al. reported that these apoJ and apoE3 might share a common binding site on megalin [9]. Therefore, it was considered that the apoE3 and apoJ might potentially impede aminoglycoside uptake as initially hypothesized. To ascertain the inhibitory effect of apoE3 on GMC binding or subsequent uptake, we examined [^{3}H] gentamicin uptake study in the presence of apoE3 or unlabeled GMC in LLC-PK_1 cells (Fig. 4). As a result, 4.3 μg/ml of apoE3 showed an inhibitory effect on [^{3}H] gentamicin uptake both in subconfluent and in confluent cell culture (Fig. 4), and the addition of unlabeled GMC resulted in a significant reduction. However, in contrast to the dramatic restoration of reduction in AMG uptake, the addition of neither apoE3 nor unlabeled GMC shows a striking reduction in [^{3}H] gentamicin uptake. Moestrup et al. has suggested that extracellular acidic phospholipids may interact with polybasic aminoglycosides as an initial epithelial binding site [19]. Thus, [^{3}H] gentamicin potentially binds to extracellular surface of the cells independent of subsequent intracellular uptake via endocytic receptor. Additionally, to ascertain the direct influence of apoE3 on GMC, we examined whether apoE3 binds to GMC. However, we could not find any evidence for a direct binding of apoE3 to GMC (data not shown). These results indicate that the protective effect may mainly depend on the disturbance of [^{3}H] gentamicin uptake into the cells by apoE3.

A variety of ligands have been found for megalin such as vitamin binding proteins, apolipoproteins and polybasic drugs, which include aminoglycosides and polymixin B [4,9]. At least in part, these exogenous ligands for megalin have been demonstrated to be carried through endocytic pathways to lysosomes [1,4,13,20]. Hence, we next studied the effect of apoE3 on GMC-dependent extracellular release of NAG, one of the lysosomal glycolytic enzymes, as a marker of renal tubular damage [20]. In consequence, treatment of cells with 4.3 μg/ml of apoE3 displayed significant improvement of GMC-dependent NAG release (Fig. 5). Previous studies demonstrated that aminoglycosides and other cationic drugs cause lysosomal dysfunctions including phospholipidosis [12,21]. Therefore, apoE3 may exert the protective effect by interfering with the binding of aminoglycoside to the site of megalin. While we could not detect the expression of megalin using a commercially available antibody, Malzoro et al. demonstrated that LLC-PK_1 is expressing megalin [22]. Even though we did not detect the expression of megalin, there is a possibility that apoE3 might protect the cells from GMC-induced NAG release related to lysosomal destabilization, which includes intracellular phospholipidosis as a consequence of reduction in GMC uptake, and would coincidentally or subsequently improve SGLT1 activity in LLC-PK_1 cells.

In conclusion, we demonstrated that apoE3 protects LLC-PK_1 cells from the reduction in SGLT1 activity. ApoE3 thus could be a valuable tool for the prevention of aminoglycoside nephrotoxicity.

References

[1] C. Schmitz, J. Hilpert, C. Jacobsen, C. Boensch, E.I. Christensen, F.C. Luft, T.E. Willnow, Megalin deficiency offers protection from renal aminoglycoside accumulation, J. Biol. Chem. 277 (2002) 618–622.
[2] K. Inui, H. Saito, R. Hori, The use of kidney epithelial cell line (LLC-PK_1) to study aminoglycoside nephrotoxicity, Dev. Toxicol. Environ. Sci. 14 (1986) 217–226.
[3] J. Nagai, H. Tanaka, N. Nakanishi, T. Murakami, M. Takano, Role of megalin in renal handling of aminoglycosides, Am. J. Physiol., Renal. Physiol. 281 (2001) F337–F344.
[4] E.I. Christensen, T.E. Willnow, Essential role of megalin in renal proximal tubule for vitamin homeostasis, J. Am. Soc. Nephrol. 10 (1999) 2224–2236.

[5] M.M. Sousa, A.G.W. Norden, C. Jacobsen, T.E. Willnow, E.I. Christensen, R.V. Thakker, P.J. Verroust, S.K. Moestrup, M.J. Saraiva, Evidence for the role of megalin in renal uptake of transthyretin, J. Biol. Chem. 275 (2000) 38176–38181.
[6] G. Zheng, D.R. Bachinsky, I. Stamenkovic, D.K. Strickland, D. Brown, G. Andres, R.T. McCluskey, Organ distribution in rats of two members of the low-density lipoprotein receptor gene family, gp330 and LRP/α2MR, and the receptor-associated protein (RAP), J. Histochem. Cytochem. 42 (1994) 531–542.
[7] I. Veinbergs, E. Van Uden, M. Mallory, M. Alford, C. McGiffert, R. DeTeresa, R. Orlando, E. Masliah, Role of apolipoprotein E receptors in regulating the differential in vivo neurotrophic effects of apolipoprotein E, Exp. Neurol. 170 (2001) 15–26.
[8] A.D. Tagalakis, I.R. Graham, D.R. Riddell, J.G. Dickson, J.S. Owen, Gene correction of the apolipoprotein (apo) E2 phenotype to wild-type apoE3 by in situ chimeraplasty, J. Biol. Chem. 276 (2001) 13226–13230.
[9] M.Z. Kounnas, E.B. Loukinova, S. Stefansson, J.A.K. Harmony, B.H. Brewer, D.K. Strickland, W.S. Argraves, Identification of glycoprotein 330 as an endocytic receptor for apolipoprotein J/clusterin, J. Biol. Chem. 270 (1995) 13070–13075.
[10] K. Takamoto, M. Kawada, T. Usui, M. Ishizuka, D. Ikeda, Aminoglycoside antibiotics reduce glucose reabsorption in kidney through down-regulation of SGLT1, Biochem. Biophys. Res. Commun. 308 (2003) 866–871.
[11] K. Kiyomiya, N. Matsushita, S. Matsuo, M. Kurebe, Differential toxic effects of gentamicin on cultured renal epithelial cells (LLC-PK_1) on application to the brush border membrane or the basolateral membrane, J. Vet. Med. Sci. 62 (2000) 971–975.
[12] R. Hori, K. Yamamoto, H. Saito, M. Kohno, K. Inui, Effect of aminoglycoside antibiotics on cellular functions of kidney epithelial cell line (LLC-PK_1): a model system for aminoglycoside nephrotoxicity, J. Pharmacol. Exp. Ther. 230 (1984) 742–748.
[13] F.M. Van't Hooft, G.M. Dallinga-Thie, A. Van Tol, Leupeptin as a tool for the detection of the sites of catabolism of rat high-density lipoprotein apolipoproteins A-I and E, Biochim. Biophys. Acta 838 (1985) 75–84.
[14] R.A. Girton, D.P. Sundin, M.E. Rosenberg, Clusterin protects renal tubular epithelial cells from gentamicin-mediated cytotoxicity, Am. J. Physiol., Renal. Physiol. 282 (2002) F703–F709.
[15] A. Blais, J. Morvan-Baleynaud, G. Friedlander, C. Le Grimellec, Primary culture of rabbit proximal tubules as a cellular model to study nephrotoxicity of xenobiotics, Kidney Int. 44 (1993) 13–18.
[16] K. Takamoto, M. Kawada, T. Usui, D. Ikeda, M. Ishizuka, T. Takeuchi, Inhibitory activity of dome formation in LLC-PK_1 cells is a selective index of aminoglycoside nephrotoxicity, J. Antibiot. 55 (2002) 605–606.
[17] H. Birn, J.C. Fyfe, C. Jacobsen, F. Mounier, P.J. Verroust, H. Ørskov, T.E. Willnow, S.K. Moestrup, E.I. Christensen, Cubilin is an albumin binding protein important for renal tubular albumin reabsorption, J. Clin. Invest. 105 (2000) 1353–1361.
[18] F. White, J.A.R. Nicoll, K. Horsburgh, Alterations in apoE and apoJ in relation to degeneration and regeneration in a mouse model of entorhinal cortex lesion, Exp. Neurol. 169 (2001) 307–318.
[19] S.K. Moestrup, S. Cui, H. Vorum, C. Bregengard, S.E. Bjørn, K. Norris, J. Gliemann, E.I. Christensen, Evidence that epithelial glycoprotein 330/megalin mediates uptake of polybacic drugs, J. Clin. Invest. 96 (1995) 1404–1413.
[20] M. Goto, K. Mizunashi, Calcitonin stimulates lysosomal enzyme release and uptake in LLC-PK_1 cells, J. Am. Soc. Nephrol. 10 (1999) 1640–1648.
[21] W.H. Halliwell, Cationic amphiphilic drug-induced phospholipidosis, Toxicol. Pathol. 25 (1997) 53–60.
[22] M.P. Marzolo, M.I. Yuseff, C. Retamal, M. Donoso, F. Ezquer, P. Farfan, Y. Li, G. Bu, Differential distribution of low-density lipoprotein-receptor-related protein (LRP) and megalin in polarized epitherial cells is determined by their cytoplasmic domains, Traffic 4 (2003) 273–288.

ELSEVIER

International Immunopharmacology 5 (2005) 281–288

International Immunopharmacology

www.elsevier.com/locate/intimp

Involvement of doxorubicin-induced Fas expression in the antitumor effect of doxorubicin on Lewis lung carcinoma in vivo

Yuya Yoshimoto, Manabu Kawada*, Daishiro Ikeda, Masaaki Ishizuka

Drug Development Unit, Numazu Bio-Medical Research Institute, Microbial Chemistry Research Center, 18-24 Miyamoto, Numazu-shi, Shizuoka 410-0301, Japan

Received 23 September 2004; accepted 23 September 2004

Abstract

Deficiency of Fas expression is one of mechanisms involved in the immune evasion by tumors. Several antitumor drugs, such as doxorubicin (DOX) increase Fas expression in tumor cells and sensitize the cells to Fas-mediated apoptosis in vitro. However, the significance of the Fas expression in vivo is still unclear. Therefore, we examined a role of Fas expression on antitumor effect of DOX using a syngeneic tumor model of Lewis lung carcinoma (3LL) cells in C57BL/6-*gld* mice that lack functional Fas ligand (FasL). In vitro, anti-Fas agonistic antibody, Jo2, did not decrease a viable cell number of 3LL cells in the absence of DOX, whereas it significantly reduced the cell viability in the presence of DOX. The treatment with DOX alone at the same dose did not induce cell death. Flowcytometric analysis of Fas expression revealed that 3LL cells expressed only a marginal amount of Fas, but the treatment of the cells with DOX increased the expression of Fas in the cell surface. When splenic T cells were prepared from 3LL-bearing C57BL/6 mice, the splenic T cells significantly killed DOX-pretreated 3LL cells more than untreated 3LL cells. In the syngeneic models, DOX inhibited growth of 3LL solid tumor both in wild-type C57BL/6 mice and in Fas-deficient C57BL/6-*lpr* mice, but it failed in C57BL/6-*gld* mice, suggesting that the interaction between host FasL and tumor Fas is involved in the antitumor effect of DOX. Furthermore, Fas expression was increased in the solid tumor by the treatment of DOX. These results suggest that the antitumor effect of DOX is partly exerted by the Fas expression and host immune defense.

Keywords: Fas; Fas ligand; Adriamycin; Chemotherapy; Tumor immunity

1. Introduction

Fas (CD95/APO-1) is a type-I membrane protein and a member of tumor necrosis factor receptor family. Binding of its intrinsic ligand, Fas ligand (FasL), to Fas induces apoptotic signaling [1,2]. Recent studies have demonstrated that Fas is down-regulated in some

* Corresponding author. Tel.: +81 55 924 0601; fax: +81 55 922 6888.
E-mail address: numazu@bikaken.or.jp (M. Kawada).

1567-5769/$ - see front matter © 2004 Elsevier B.V. All rights reserved.
doi:10.1016/j.intimp.2004.09.032

human malignancies, including lung, breast, and esophageal cancer [3–5]. Deficiency of Fas expression should contribute to escape from host immune surveillance in those tumor cells because Fas/FasL interaction is involved in the cytolysis of the tumor cells mediated by cytotoxic T lymphocytes (CTLs) [6,7]. Fas expression is in fact shown as a significant prognostic factor in the human malignancies [3–5], and it is demonstrated that Fas overexpression on solid tumor cells delays the tumor growth in vivo in a syngeneic model [8]. Therefore, sensitization of tumor cells to CTLs by restoring Fas expression will be a practical approach to cancer treatment.

It has been reported that several antitumor drugs enhance susceptibility of tumor cells to Fas-mediated apoptosis [9–11]. Recently, Kataoka et al. [12] have shown that DNA-damaging agent, such as doxorubicin (DOX), sensitizes murine thymoma EL-4 cells to Fas-mediated apoptosis via an increase in the expression of Fas on the cell surface. These findings arise a possibility that the chemotherapeutic effect of antitumor drugs used clinically is mediated by the Fas expression and altered susceptibility to CTL-mediated cytolysis of tumor cells. However, significance of the Fas expression by the drugs on antitumor effect in vivo is still unclear. In the present study, we have defined the role of DOX-induced Fas expression on its antitumor effect using a syngeneic model of 3LL cells in FasL-deficient C57BL/6-*gld* mice [13].

2. Materials and methods

2.1. Cell line and susceptibility to Fas stimuli

3LL cells (Lewis lung carcinoma, H-2^b) were grown in Dulbecco's modified Eagle's medium (Nissui, Ohita, Japan) supplemented with 10% fetal bovine serum (JRH Biosciences, Lenexa, KS), 100 U/ml of penicillin G, and 0.1 mg/ml of streptomycin at 37 °C in a 5% CO_2–95% air atmosphere. To examine the susceptibility to Fas-mediated apoptosis, the cells were treated with an agonistic anti-Fas antibody (clone Jo2, BD Bioscience, Stockholm, Sweden) in the presence or absence of DOX for 48 h. After the adherent and detached cells were combined together, the cells were stained with 0.2% trypan blue, and the percentage of viable cells was determined using a hemocytometer. Cell viability [%] means the ratio of number of trypan blue impermeable cells in total cell counts (number of both trypan blue impermeable and permeable cells).

2.2. Detection of cell surface expression of Fas and FasL

Cells were detached from plastic culture plates using 5 mM EDTA in PBS and then were incubated with 8 μg/ml of the appropriate antibody (for Fas, clone Jo2; for FasL, clone MFL3, BD Bioscience) for 1 h at 4 °C. The cells were washed and then incubated with 10 μg/ml of a secondary antibody labeled with FITC (Jackson ImmunoResearch, West Grove, PA). After washing, 30,000 cells were analyzed by a flowcytometer (FACScalibur, BD Systems).

2.3. CTL cytolysis assay

3LL-bearing C57BL/6 mice were sacrificed, and nylon-wool-passed splenic T cells were prepared. Target 3LL cells pretreated with or without 0.3 μg/ml of DOX for 24 h were labeled with ^{51}Cr ($Na_2^{51}CrO_4$, 14.3 GBq/mg, NEN, Boston, MA) and then incubated with the splenic T cells at the indicated ratios for 20 h. After incubation, the supernatant was collected, and ^{51}Cr radioactivity was counted in a gamma counter (ARC-300, ALOKA, Tokyo, Japan). After the disruption of the target cells by 1% SDS, the maximum counts in the target cells were determined. The mean percentage of specific cytolysis was calculated as follows: %cytolysis=[(test count−spontaneous count)/(maximum count−spontaneous count)]×100. Maximum count and spontaneous count were 737±33.8 and 290±12.9 cpm for control 3LL cells and 1422±96 and 497±18 cpm for DOX-treated 3LL cells, respectively. Although the counts in the DOX-treated 3LL cells were higher than that in the untreated 3LL cells, the ratios of spontaneous count/maximum count were almost the same.

2.4. Detection of expression of Fas mRNA by RT–PCR

Total RNA was extracted from tumor cells by using an RNeasy kit (Qiagen, Hilden, Germany) and reverse transcribed to cDNA using Reverse Transcription System (Promega, Madison, WI) kit according to

the manufacturers' instructions. cDNA was amplified by the following primers and conditions: Fas, 5′-ATGCACACTCTGCGATGAAG-3′ (sense) and 5′-TTCAGGGTCATCCTGTCTCC-3′ (antisense), 30 cycles of 94 °C for 1 min, 58 °C for 40 s, 72 °C for 40 s; GAPDH, 5′-GGTGAAGGTCGGTGTGAACGGA-3′ (sense) and 5′-TGTTAGTGGGGTCTCGCTCCTG-3′ (antisense), 15 cycles of 94 °C for 1 min, 58 °C for 40 s, 72 °C for 40 s. PCR products (Fas, 313 bp; GAPDH, 221 bp) were analyzed by 2% agarose gels and stained with SYBR Green I (Takara, Shiga, Japan).

To detect expression of Fas in vivo, 6-week-old female C57BL/6J-*lpr/lpr* mice [14] (Japan SLC, Shizuoka, Japan) were inoculated subcutaneously (s.c.) with 5×10^5 of 3LL cells. DOX was injected intraperitoneally (i.p.) when the tumor volume was reached at 100 mm^3 (day 8 after tumor inoculation), and the mice were sacrificed, and the 3LL solid tumors were obtained at day 9.

2.5. Experimental chemotherapy

C57BL/6J (H-2^b), C57BL/6J-*lpr/lpr* (H-2^b), and C57BL/6J-*gld/gld* (H-2^b) mice were purchased from Japan SLC, and maintained in a specific pathogen-free barrier facility. Six-week-old female mice were inoculated s.c. with 5×10^5 of Lewis lung carcinoma 3LL cells (H-2^b) at day 0. DOX was injected i.p. Diameters of the tumors were measured every other day with calipers, and the volume was calculated by the formula, tumor volume=(longest diameter)$\times$(shortest diameter)$^2\times1/2$. When the tumor volumes of control group were reached at 1000 mm^3, the mice were sacrificed, and the tumor weights were measured. Statistical significance was analyzed by Student's *t*-test, and differences were considered statistically significant at $P<0.05$.

3. Results

3.1. Doxorubicin-induced Fas expression and enhanced sensitivity to Fas-mediated apoptosis in vitro

First, we examined whether DOX sensitizes 3LL cells to Fas-mediated apoptosis in vitro. 3LL cells

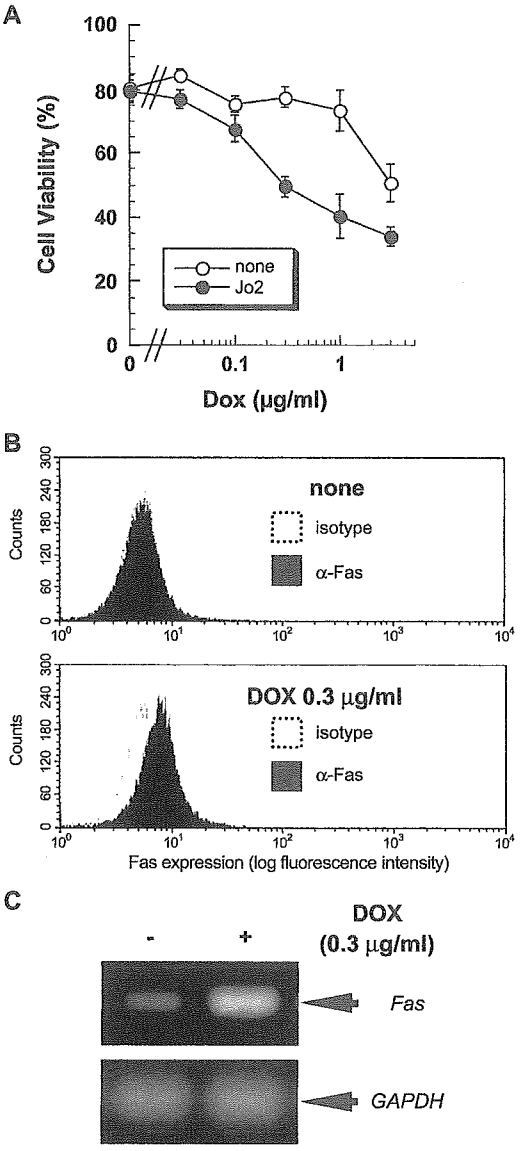

Fig. 1. DOX-induced Fas expression and enhanced sensitivity. (A) Sensitivity to Fas stimuli. Cells were treated with an agonistic anti-Fas antibody (clone Jo2, 1 μg/ml) in the presence or absence of the indicated concentrations of DOX for 48 h. After adherent and detached cells were combined together, the cells were stained with 0.2% trypan blue, and the percentage of viable cells was determined using a hemocytometer. Values are means for quadruplicate determinations; bars, S.D. (B) Cell surface Fas expression. Cells treated with 0.3 μg/ml of DOX for 24 h were recovered and stained with anti-Fas antibody, immune fluorescence was quantified by flowcytometric analysis. (C) Fas mRNA expression. Cells were treated with 0.3 μg/ml of DOX for 24 h. mRNA expression was analyzed by RT–PCR.

treated with or without DOX were incubated with 1 μg/ml of anti-Fas agonistic antibody, Jo2, for 48 h, and their viability was assessed by trypan blue dye exclusion assay. As shown in Fig. 1A, DOX did not decrease a viable cell number up to 1 μg/ml in the absence of Jo2. But, it significantly reduced the cell viability to 40% in the presence of Jo2. The treatment with Jo2 alone did not induce cell death. Flowcytometric analysis of Fas expression revealed that 3LL cells expressed only a marginal amount of Fas, but treatment of the cells with DOX (0.3 μg/ml) caused an increase in the expression of Fas on the cell surface (Fig. 1B). In addition, expression of Fas mRNA was up-regulated by treatment with DOX (Fig. 1C). When splenic T cells were prepared from 3LL-bearing C57BL/6 mice, the splenic T cells significantly killed DOX-pretreated 3LL cells more than untreated 3LL cells (Fig. 2). These results indicate that DOX induces Fas expression in 3LL cells and enhances sensitivity to Fas-mediated apoptosis. FasL expression in 3LL cells was also examined by a flowcytometer; however, it was at a marginal level, and the expression level was not changed by the treatment with DOX (data not shown).

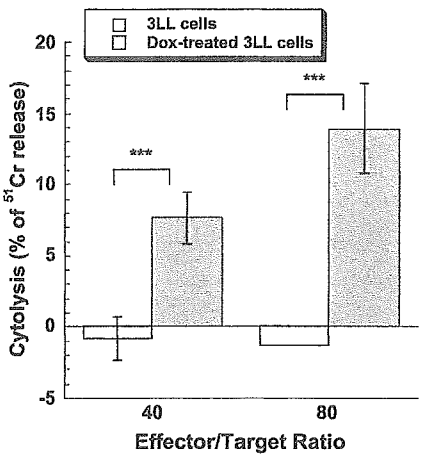

Fig. 2. Doxorubicin-induced sensitization of 3LL cells to cytotoxic activity of CTL. 3LL-bearing C57BL/6 mice were sacrificed, and splenic T cells were prepared. Target 3LL cells pretreated with or without 0.3 μg/ml of DOX for 24 h were labeled with ^{51}Cr and then incubated with the splenic T cells at the indicated ratios for 20 h. After incubation, the supernatant was collected, and ^{51}Cr radioactivity was counted in a gamma counter. Values are means for triplicate determinations; bars, S.D. ***$P<0.005$ in comparison with control group.

3.2. Doxorubicin-induced Fas expression in vivo and its role on the antitumor effect

Our current working hypothesis is that the antitumor effect of DOX in vivo would be attributed to not only its direct antiproliferative effect but also host immune defense through enhancement of Fas expression in tumor cells because CTL-mediated cytolysis of tumor cells mainly occurs via Fas-mediated apoptosis [6,7]. We tested this hypothesis using a syngeneic tumor model of 3LL cells in FasL-deficient C57BL/6-*gld* mice [13] in which CTL-mediated cytolysis via Fas did not occur. 3LL cells were inoculated into *gld* mice, and the mice were treated with DOX, and then inhibition of the tumor growth in the *gld* mice was compared with that in C57BL/6 (wild type) mice. It was reported that certain antitumor drugs can eliminate immune suppressor cells and augment antitumor immune responses [15,16], and that apoptosis of thymocytes in vivo by antitumor drugs occurs through activation of Fas/FasL system [17]. Thus, there is a possibility that deficiency of Fas/FasL system in *gld* mice affects the DOX-induced modification of antitumor immune responses. To clarify this point, Fas-deficient C57BL/6-*lpr* mice carrying *lpr* mutation in Fas gene [14] were also used for this experiment in addition to the two strains. The *lpr*-derived deficiency of Fas/FasL system affects immune system in *lpr* mice, as well as that in *gld* mice [17–20].

3LL cells were inoculated s.c. into syngeneic C57BL/6 (wild type) mice, C57BL/6-*lpr* mice, or C57BL/6-*gld* mice, and then the tumor growth was measured. DOX was administered i.p. at days 1–5, 7–11, and 14–16. As shown in Fig. 3A, the treatment with DOX showed no significant antitumor effect in *gld* mice, while it exhibited inhibition of the tumor growth both in wild-type C57BL/6 mice and in *lpr* mice. Decrease in the tumor weights by DOX was significant in wild-type group and *lpr* group. However, no significant decrease in the tumor weight was observed in *gld* group (Fig. 3B). This result clearly demonstrates that the antitumor effect of DOX in vivo is exerted by the mechanisms through host FasL.